

Inhomogeneous Double Thinning—Modeling and Analysis of Cellular Networks by Using Inhomogeneous Poisson Point Processes

Marco Di Renzo¹, Senior Member, IEEE, Shanshan Wang, and Xiaojun Xi

Abstract—In this paper, we introduce a new methodology for modeling and analyzing downlink cellular networks, where the base stations (BSs) constitute a motion-invariant point process (PP) that exhibits some degree of interactions among the points, i.e., spatial repulsion or spatial clustering. The proposed approach is based on the theory of inhomogeneous Poisson PPs (I-PPPs) and is referred to as inhomogeneous double thinning (IDT) approach. In a PP, the distribution of the distance from a randomly distributed (typical) user to its nearest BS depends on the degree of spatial repulsion or clustering exhibited by the PP. In addition, the average number of interfering BSs that lies within a given distance from the typical user is a function of the repulsion and clustering characteristics of the PP. The proposed approach consists of approximating the original motion-invariant PP with an equivalent PP that is made of the superposition of two conditionally independent I-PPPs. The inhomogeneities of both PPs are created from the point of view of the typical user (“user-centric”): the first one is based on the distribution of the user’s distance to its nearest BS and the second one is based on the distance-dependent average number of interfering BSs around the user. The inhomogeneities are mathematically modeled through two distance-dependent thinning functions and a tractable expression of the coverage probability is obtained. Sufficient conditions on the parameters of the thinning functions that guarantee better or worse coverage compared with the baseline homogeneous PPP model are identified. The accuracy of the IDT approach is substantiated with the aid of empirical data for the spatial distribution of the BSs.

Index Terms— Cellular networks, stochastic geometry, inhomogeneous point processes, spatial inhibition, and spatial clustering.

I. INTRODUCTION

IN THE last few years, the theory of Poisson Point Processes (PPPs) has been extensively employed for modeling, analyzing, and optimizing the performance of emerging cellular network architectures [1]. Notable examples include, Heterogeneous Cellular Networks (HCNs) [2], [3],

Manuscript received October 21, 2017; revised March 16, 2018; accepted May 9, 2018. Date of publication May 28, 2018; date of current version August 10, 2018. This work was supported in part by the European Commission through the H2020-MSCA ETN-5Gwireless Project under Grant 641985 and in part by the H2020-MSCA ETN-5Gaura Project under Grant 675806. The associate editor coordinating the review of this paper and approving it for publication was L. K. Rasmussen. (Corresponding author: Marco Di Renzo.)

The authors are with the Laboratoire des Signaux et Systèmes, CNRS, CentraleSupélec, Univ Paris Sud, Université Paris-Saclay, 91192 Gif-sur-Yvette, France (e-mail: marco.direnzo@l2s.centralesupelec.fr; shanshan.wang@l2s.centralesupelec.fr; xiaojun.xi@l2s.centralesupelec.fr).

Color versions of one or more of the figures in this paper are available online at <http://ieeexplore.ieee.org>.

Digital Object Identifier 10.1109/TWC.2018.2838597

Multiple-Input-Multiple-Output (MIMO) HCNs [4], [5], millimeter-wave cellular HCNs [6], [7], and massive MIMO cellular networks [8]. Recently, comprehensive mathematical frameworks for taking into account the impact of spatial blockages, antenna radiation patterns, and the network load have been introduced [9] and empirically validated [10]. Surveys and tutorials on the application of PPPs to the modeling and analysis of HCNs are available in [11]–[14].

A. Beyond the Poisson Point Process Model: State-of-the-Art and Limitations

Modeling cellular networks by using PPPs has the inherent advantage of mathematical tractability. Empirical evidence suggests, however, that practical cellular network deployments are likely to exhibit some degree of interactions among the locations of the Base Stations (BSs), which include spatial inhibition, i.e., repulsion [15], and spatial aggregation, i.e., clustering [16]. More recently, several other spatial models have been proposed for overcoming the complete spatial randomness property of PPPs, i.e., their inherent limitation of modeling spatial correlations [17]–[29]. In [17], Matérn PPs are used for modeling cellular networks that exhibit spatial repulsion. In [18] and [19], the author introduces the AS-PPP (ASAPPP) approach, which consists of obtaining the coverage probability of repulsive PPs through a right-shift of the coverage probability under the PPP model. The right-shift to be applied is termed (asymptotic) deployment gain. General results on the existence and computation of the asymptotic deployment gain are available in [21] and [25]. The ASAPPP method is generalized for application to HCNs in [24]. In [20], the Ginibre PP (GPP) is proposed for modeling repulsive cellular networks in urban and rural environments. Further experimental validation of the suitability of GPPs is available in [22]. In [23], Determinantal PPs (DPPs) are investigated and their accuracy is substantiated with the aid of practical network deployments. In [26], the Poisson Hole Process (PHP) is proposed to model the spatial interactions in cognitive and device-to-device networks. In [27], the Log-Gaussian Cox Process (LGCP) is proposed, based on empirical data, to account for the spatial correlation arising in multi-operator cellular networks. In [28], a cellular network model constituted by the superposition of a shifted lattice PP and a PPP is introduced, by bridging the gap between completely regular and totally random networks. In [29], a general class of Poisson cluster PPs is studied for modeling the spatial

coupling between different tiers of HCNs. The Matérn Cluster PP (MCP) is used, e.g., for modeling the locations of small-cell BSs.

By carefully analyzing all the above-mentioned proposals for modeling cellular networks via non-PPPs, two main conclusions can be drawn: 1) non-PPPs are more accurate than PPPs for modeling emerging cellular architectures and 2) the price to pay is the loss of mathematical tractability and the limited design insight that can be obtained from the resulting frameworks. As far as the computation of the coverage probability is concerned, among all the available approaches, the ASAPP method is certainly the most tractable. The asymptotic deployment gain, however, may not be always explicitly computable [21, Lemma 4]. The approaches proposed so far are, in addition, PP-specific: Each spatial PP results in a different formulation of the coverage probability. Therefore, there is a compelling need for a unified and tractable methodology for modeling cellular networks that exhibit spatial repulsion and/or clustering.

B. On Modeling Motion-Invariant PPs via I-PPPs:

Rationale, Interpretation, and Challenge

Motivated by these considerations, we study the suitability of Inhomogeneous PPPs (I-PPPs) for modeling cellular networks that exhibit spatial repulsion and clustering. Before proceeding further, three main questions need to be addressed: 1) *What is the rationale of using I-PPPs for modeling cellular networks?* 2) *I-PPPs are non-stationary PPs – How to interpret them for analyzing the typical user?* 3) *What are the modeling challenges for leveraging I-PPPs?*

1) *Rationale:* Three reasons motivate us to analyze the suitability of I-PPPs for system-level modeling and analysis of cellular networks. 1) Since there are many possible causes at the origin of the spatial correlation in PPs, empirical evidence shows that inhibition and aggregation may be difficult to be disentangled from spatial inhomogeneity [30, Sec. 7.3.5.2]. In addition, the inherent inhomogeneity of the spatial distribution of users, who may be concentrated in hotspots, buildings, malls, pedestrian zones, etc., highly determines the resulting spatial correlation of cellular BSs [31]. In other words, there is a strong dependence between the spatial distribution of the network traffic, which is inhomogeneous, and the actual deployment of cellular BSs. 2) I-PPPs inherit all the main properties of Homogeneous PPPs (H-PPPs) that make them mathematically tractable [32, Sec. 2]. Hence, I-PPPs are the most tractable alternative to PPPs. 3) Recent studies on uplink cellular networks have put forth the I-PPPs as a suitable approximation for modeling the otherwise intractable spatial correlations that characterize the locations of the users scheduled for transmission on the same physical channel [33], [34]. We use a similar line of thought for approximating both repulsion and clustering among the locations of cellular BSs.

2) *Interpretation:* The spatial models proposed in [17]–[29] are based on motion-invariant PPs. Hence, the PPs are invariant under translations (i.e., are stationary) and rotations around the origin (i.e., are isotropic) [35], [36]. This implies that, e.g., the coverage probability of a randomly distributed (typical) user is independent of its actual location. For this

reason, the typical user is always assumed to be at the origin [17]–[29]. I-PPPs, on the other hand, are non-stationary PPs and the performance of a randomly chosen user depends on its actual location, i.e., on the “panorama” or view that the user has of the network. Bearing this difference in mind, the proposed approach has an unambiguous interpretation: It consists of *approximating* a motion-invariant PP, e.g., one of those in [17]–[29], with an equivalent I-PPP whose inhomogeneity is created from the point of view of the typical user of the original motion-invariant PP, e.g., the user located at the origin. In simple terms, we approximate a motion-invariant PP with an equivalent I-PPP, where “equivalent” means that the network’s view of the typical user located at the origin of the original motion-invariant PP is (approximately) the same as the network’s view of a probe user located at the origin¹ of the equivalent I-PPP. The equivalency of the network’s panoramas is obtained by appropriately choosing the spatial inhomogeneity of the equivalent I-PPP as a function of the spatial inhibition and aggregation properties of the original motion-invariant PP.

3) *Challenge:* I-PPPs are more mathematically tractable than PPs that exhibit spatial repulsion and clustering [32, Sec. 2]. I-PPPs may, however, be more difficult to handle [31]. Let us consider, e.g., GPPs [20] and DPPs [23]. They are uniquely determined by one or two *distance-independent parameters* that are simple to be estimated based on empirical data. I-PPPs necessitate, on the other hand, the definition of a *distance-dependent intensity function*, whose choice is a non-trivial challenge as no a priori information on its structure exists to date. Its definition, in addition, needs to account for the critical balance between modeling accuracy and mathematical tractability.

In summary, the specific intention of the present paper is to study whether I-PPPs are suitable for modeling practical cellular network deployments and whether tractable analytical frameworks can be obtained, even though, compared with other PPs, I-PPPs may be more difficult to fit from empirical data. An important contribution of the present paper is, in addition, to introduce tractable yet accurate distance-dependent intensity functions and to propose a simple approach for estimating their parameters from empirical data sets that correspond to practical cellular network deployments.

C. Inhomogeneous Double Thinning: Novelty and Contribution

The proposed approach based on I-PPPs is referred to as Inhomogeneous Double Thinning (IDT) approach. The specific novelty and contributions made by the present paper are as follows.

- For the first time, we propose I-PPPs for modeling the spatial correlations inherently present in cellular network deployments. The IDT approach is general and flexible enough for modeling cellular networks that exhibit spatial

¹It is worth mentioning that the origin is chosen only for ease of analysis and modeling, any other locations may be considered for the probe user provided that the spatial inhomogeneity is created accordingly.

TABLE I
SUMMARY OF MAIN SYMBOLS AND FUNCTIONS USED THROUGHOUT THE PAPER

Symbol/Function	Definition
$\mathbb{E}\{\cdot\}, \Pr\{\cdot\}$	Expectation operator, probability measure
$\mathbb{E}_{\Psi}^{!x_0}\{\cdot\}$	Expectation of point process Ψ under the reduced Palm measure
$\lambda_{BS}, \lambda_{MT}$	Density of base stations, mobile terminals
$\Psi_{BS}, \Psi_{BS}^{(1)}$	Motion-invariant point process of base stations, interfering base stations
$\Phi_{BS}, \Phi_{BS}^{(1)}$	Inhomogeneous Poisson point process of base stations, interfering base stations
BS_0, x_0	Serving base station, location of the serving base station
P_{tx}, σ_N^2	Transmit power, noise power
x, u	Generic location of a base station, mobile terminal
$ x - u , g_x$	Distance between locations x and u , fading power gain at location x
$\ y - \Psi\ $	Minimum distance between location y and point process Ψ
$l(\cdot), L_x, L_0$	Path-loss, shorthand of the path-loss at location x , path-loss of the intended link
$\kappa, \gamma > 2$	Path-loss constant, slope (exponent)
$R_{cell} = \sqrt{1/(\pi\lambda_{BS})}, R_A$	Average cell radius, maximum radius of the network
$F_{\Psi}(\cdot), K_{\Psi}(\cdot)$	F-function, non-regularized Ripley's K-function of point process Ψ
$\mathcal{B}(x, r), \Lambda_{\Phi}(\cdot)$	Ball of center x and radius r , intensity measure of point process Φ
$f_X(\cdot), \mathcal{M}_{1,X}(\cdot)$	Probability density function of X , Laplace functional conditioned on X
$\mathbb{1}(\cdot), {}_2F_1(\cdot, \cdot, \cdot, \cdot)$	Indicator function, Gauss hypergeometric function
$\max\{x, y\}, \min\{x, y\}$	maximum, minimum between x and y
$\Upsilon^{(1)}(r; \cdot)$	First-order derivative of $\Upsilon(r; \cdot)$ with respect to r
$(a_F, b_F, c_F), (a_K, b_K, c_K)$	Parameters of the approximating inhomogeneous Poisson point processes

inhibition, aggregation, as well as cellular networks where some BSs may exhibit spatial inhibition and some other BSs may exhibit spatial aggregation (e.g., a multi-tier cellular network where the first and second tiers of BSs are distributed according to, e.g., a GPP or DPP and a LGCP or MCPP, respectively).

- We introduce two distance-dependent intensity functions to create the inhomogeneities based on spatial inhibition and aggregation properties empirically observed in practical cellular networks. They are shown to yield a good trade-off between accuracy and tractability.
- We devise a method for approximating the network's panorama of the typical user of the original motion-invariant PP with the network's panorama of a probe user located at the origin of the equivalent I-PPP. The essence of the method is as follows. In a motion-invariant PP, the distribution of the distance from the typical user to its nearest BS (the F-function [30, Sec. 8.3]) and the average number of interfering BSs within a given distance from the typical user (related to the Ripley's K-function [30, Sec. 7.3]) depend on the degree of spatial inhibition and aggregation exhibited by the PP. The IDT approach approximates the original motion-invariant PP with an equivalent I-PPP that is the result of the superposition of two conditionally independent I-PPPs. The inhomogeneities of the first and second I-PPP are created based on the F-function and the non-regularized K-function of the original motion-invariant PP, respectively. The first I-PPP and the second I-PPP are employed for modeling the location of the serving BS and the locations of the interfering BSs, respectively.

- Based on the IDT approach, a new tractable analytical expression of the coverage probability of cellular networks is introduced. The approach is generalized for application to cellular networks with spatial-dependent blockages [9] and multi-tier deployments [3].
- The analytical frameworks of the coverage probability obtained from H-PPP and I-PPP modeling approaches are compared against each other. Notably, sufficient conditions on the parameters of the proposed thinning functions that guarantee a better or worse coverage probability compared with the baseline H-PPP model are identified.
- The accuracy of the IDT approach is substantiated via empirical data for the locations of cellular BSs. The study unveils that the IDT approach yields accurate estimates of the coverage for several motion-invariant PPs, e.g., GPPs, DPPs, LGCPs, PHPs, MCPPs, and lattice PPs.

D. Paper Organization and Structure

The rest of the present paper is organized as follows. In Section II, the system model is presented. In Section III, the IDT approach is introduced. In Section IV, the analytical framework of the coverage probability is provided. In Section V, the IDT approach is generalized for application to spatial-dependent blockage models and multi-tier deployments. In Section VI, the IDT approach is substantiated via empirical data and simulations. Finally, Section VII concludes this paper.

Notation: The main symbols and functions used in this paper are reported in Table I.

II. SYSTEM MODEL

In this section, the network model is introduced. We focus our attention on single-tier cellular networks, by assuming an unbounded path-loss model and neglecting spatial blockages [9]. System models with blockages and multi-tier deployments are discussed in Section V.

A. Cellular Networks Modeling

A downlink cellular network is considered. The BSs are modeled as points of a motion-invariant PP, denoted by Ψ_{BS} , of density λ_{BS} . The locations of BSs are denoted by $x \in \Psi_{\text{BS}} \subseteq \mathbb{R}^2$. The Mobile Terminals (MTs) are distributed independently of each other and uniformly at random in \mathbb{R}^2 . The density of MTs is denoted by λ_{MT} . Thanks to the assumption of motion-invariance, the PP of BSs is stationary and isotropic. As a result, the analytical frameworks are developed for the typical MT, denoted by MT_0 , that is located at the origin. The BS serving MT_0 is denoted by BS_0 . Its location is denoted by $x_0 \in \Psi_{\text{BS}}$. The cell association criterion is introduced in Section II-C. Examples of PPs that satisfy these assumptions are reported in [20], [23], and [26]–[29].² The BSs and MTs are equipped with a single omnidirectional antenna. Each BS transmits with a constant power denoted by P_{tx} . A fully loaded assumption is considered, i.e., $\lambda_{\text{MT}} \gg \lambda_{\text{BS}}$, which implies that all the BSs are active and have MTs to serve. These latter assumptions may be removed based on [9]. This is not considered, however, in the present paper, in order to keep the focus on the new approach for modeling the spatial distribution of the BSs. All available BSs transmit on the same physical channel as BS_0 . The PP of interfering BSs is denoted by $\Psi_{\text{BS}}^{(1)}$. Besides the inter-cell interference, Gaussian noise with power σ_{N}^2 is taken into account as well.

B. Channel Modeling

For each BS-to- MT_0 link, path-loss and fast-fading are considered. Shadowing is not explicitly considered for simplicity, but it can be taken into account by using the approach in [9]. All BS-to- MT_0 links are assumed to be mutually independent and identically distributed (i.i.d.).

1) *Path-Loss*: Consider a generic BS whose location is $x \in \Psi_{\text{BS}}$. The path-loss is defined as $l(x) = \kappa \|x\|^\gamma$, where κ and $\gamma > 2$ are the path-loss constant and the path-loss slope (exponent).

2) *Fast-Fading*: Consider a generic BS-to- MT_0 link. The power gain due to small-scale fading is assumed to follow an exponential distribution with mean m . Without loss of generality, $m = 1$ is assumed. The power gain of a generic BS-to- MT_0 link is denoted by g_x for $x \in \Psi_{\text{BS}}$.

C. Cell Association Criterion

A cell association criterion based on the highest average received power is assumed. Let $x \in \Psi_{\text{BS}}$ be the location

²As discussed in [15, Sec. II-E], the lattice is not a stationary PP. However, it can be made stationary by introducing a random translation over the Voronoi cell of the origin. Another option is to consider the concept of empirical homogeneity condition [39, Sec. III]. Either way, the methods discussed and the conclusions drawn in the present paper apply unaltered.

of a generic BS. The location, x_0 , of the serving BS, BS_0 , is obtained as follows:

$$x_0 = \arg \max_{x \in \Psi_{\text{BS}}} \{1/l(x)\} = \arg \max_{x \in \Psi_{\text{BS}}} \{1/L_x\} \quad (1)$$

where $L_x = l(x)$ is a shorthand. As for the intended link, $L_0 = l(x_0) = \min_{x \in \Psi_{\text{BS}}} \{L_x\}$ holds.

D. Coverage Probability

The performance metric of interest is the coverage probability, P_{cov} , that is defined as follows:

$$P_{\text{cov}} = \Pr \left\{ \frac{P_{\text{tx}} g_0 / L_0}{\sigma_{\text{N}}^2 + \sum_{x \in \Psi_{\text{BS}}^{(1)}} P_{\text{tx}} g_x / L_x} > T \right\} \quad (2)$$

where $\Psi_{\text{BS}}^{(1)} = \Psi_{\text{BS}} \setminus x_0$.

We focus our attention on the coverage probability because it corresponds to the complementary cumulative distribution function of the SINR (Signal-to-Interference+Noise Ratio), and, thus, it completely characterizes the statistical properties of the SINR. Other relevant performance metrics, e.g., the average rate, the potential spectral efficiency, and the local delay, that depend on the SINR can be directly obtained from the coverage probability [37], [38].

Under the assumptions of this paper, P_{cov} can be formulated as shown in the following lemma.

Lemma 1: An analytical expression of the coverage probability in (2) is as follows:

$$P_{\text{cov}} = \int_0^{+\infty} \exp(-\xi T \sigma_{\text{N}}^2 / P_{\text{tx}}) \mathcal{M}_{\text{I},L_0}(\xi; T) f_{L_0}(\xi) d\xi \quad (3)$$

where $f_{L_0}(\cdot)$ is the Probability Density Function (PDF) of L_0 introduced in Section II-C and $\mathcal{M}_{\text{I},L_0}(\cdot; \cdot)$ is the Laplace functional of the PP, $\Psi_{\text{BS}}^{(1)} = \Psi_{\text{BS}} \setminus x_0$, of interfering BSs:

$$\begin{aligned} \mathcal{M}_{\text{I},L_0}(\xi = L_0 = l(x_0); T) \\ = \mathbb{E}_{\Psi_{\text{BS}}^{(1)}, x_0} \left\{ \prod_{x \in \Psi_{\text{BS}} \setminus x_0} (1 + T(\xi/l(x)))^{-1} \right\} \end{aligned} \quad (4)$$

Proof: It directly follows from [1]. \square

Remark 1: In (4), we have made explicit that the computation of the Laplace functional of the PP of interfering BSs, $\Psi_{\text{BS}}^{(1)} = \Psi_{\text{BS}} \setminus x_0$, necessitates the knowledge of the reduced Palm distribution of the PP, Ψ_{BS} [36, Sec. 8]. In simple terms, the expectation under the reduced Palm distribution, $\mathbb{E}_{\Psi_{\text{BS}}^{(1)}, x_0} \{\cdot\}$, is obtained by conditioning upon x_0 and by removing it from the PP. \square

By direct inspection of (3) and (4), we infer that the mathematical tractability of P_{cov} depends on $f_{L_0}(\cdot)$ and $\mathcal{M}_{\text{I},L_0}(\cdot; \cdot)$. In general, the following holds [35], [36]: i) $f_{L_0}(\cdot)$ depends on the Contact Distance Distribution (CDD) of the PP, Ψ_{BS} , of BSs (see *Definition 1*), and ii) $\mathcal{M}_{\text{I},L_0}(\cdot; \cdot)$ depends on the Laplace functional of the PP, $\Psi_{\text{BS}}^{(1)} = \Psi_{\text{BS}} \setminus x_0$, of interfering BSs, which requires the reduced Palm distribution of the PP,

Ψ_{BS} , of BSs to be known. The CDD and reduced Palm distribution of an arbitrary motion-invariant PP, however, may not be known or may not be mathematically tractable. The tractability of the H-PPP lies in the simple analytical expression of $f_{L_0}(\cdot)$ [39] and in the fact that the reduced Palm distribution of a H-PPP coincides with the distribution of the H-PPP itself. Other motion-invariant PPs, e.g., GPPs and DPPs, admit analytical expressions of the CDD and their reduced Palm distribution is known. Their P_{cov} has, however, a limited analytical tractability [20], [23]. In Section III, we propose a tractable analytical approach that overcomes this limitation, by leveraging the theory of I-PPPs.

E. Preliminary Definitions

For ease of exposition, we introduce a few definitions that are used in the next sections.

Definition 1: Let Ψ_{BS} be a motion-invariant PP. Let $u \in \mathbb{R}^2$ be the location of a random MT. The CDD or F-function of Ψ_{BS} at location u is $F_{\Psi_{\text{BS}}}^{(u)}(r) = \Pr\{\|u - \Psi_{\text{BS}}\| < r\} \stackrel{(a)}{=} \Pr\{\|\Psi_{\text{BS}}\| < r\} = F_{\Psi_{\text{BS}}}(r)$, i.e., it is the Cumulative Distribution Function (CDF) of the distance between u and its nearest BS in Ψ_{BS} [36, Sec. 2.8]. The equality in (a) is due to the motion invariance of Ψ_{BS} . \square

Definition 2: Let Ψ_{BS} be a motion-invariant PP. Let $x \in \Psi_{\text{BS}}$ be the generic location of a BS of Ψ_{BS} . The “non-regularized” Ripley’s function or “non-regularized” K-function of Ψ_{BS} is $K_{\Psi_{\text{BS}}}^{(x)}(r) = \mathbb{E}_{\Psi_{\text{BS}}}^{\{x\}}\{\|\Psi_{\text{BS}}\| < r\} \stackrel{(a)}{=} \mathbb{E}_{\Psi_{\text{BS}}}^{\{0\}}\{\|\Psi_{\text{BS}}\| < r\} \stackrel{(b)}{=} K_{\Psi_{\text{BS}}}(r)$, i.e., it is the average number of BSs in Ψ_{BS} that lie inside the ball of center x and radius r without counting the BS at x [36, Sec. 6.5]. The equalities in (a) and (b) are due to the motion invariance of Ψ_{BS} . \square

Remark 2: The Ripley’s K-function in *Definition 2* is non-regularized because it is not scaled by the density, λ_{BS} , of the motion-invariant PP, Ψ_{BS} [36, Sec. 6.5]. \square

Remark 3: Let Φ_{BS} be an I-PPP. The non-regularized K-function in *Definition 2* is denoted by $\Lambda_{\Phi_{\text{BS}}}(\mathcal{B}(x, r)) = K_{\Phi_{\text{BS}}}^{(x)}(r)$, where $\mathcal{B}(x, r)$ is the ball of center $x \in \Phi_{\text{BS}}$ and radius r , and $\Lambda_{\Phi_{\text{BS}}}(\cdot)$ is the intensity measure of Φ_{BS} [32, Sec. 2.2]. Since I-PPPs are non-stationary PPs, the intensity measure depends on the location x [32, Sec. 2.2]. If Φ_{BS} is a H-PPP, the non-regularized K-function is $\Lambda_{\Phi_{\text{BS}}}(\mathcal{B}(x, r)) = \Lambda_{\Phi_{\text{BS}}}(\mathcal{B}(x=0, r)) = \lambda_{\Phi_{\text{BS}}}\pi r^2$, which is independent of x . \square

Remark 4: Let Φ_{BS} be an I-PPP with intensity measure $\Lambda_{\Phi_{\text{BS}}}(\cdot)$. The CDD or F-function of Φ_{BS} at location $u \in \mathbb{R}^2$ is $F_{\Phi_{\text{BS}}}^{(u)}(r) = 1 - \exp(-\Lambda_{\Phi_{\text{BS}}}(\mathcal{B}(u, r)))$, where $\mathcal{B}(u, r)$ is the ball of center u and radius r [32, Sec. 2.2]. If Φ_{BS} is a H-PPP, the F-function is $F_{\Phi_{\text{BS}}}^{(u)}(r) = F_{\Phi_{\text{BS}}}^{(u=0)}(r) = 1 - \exp(-\lambda_{\Phi_{\text{BS}}}\pi r^2)$, which is independent of the location u . \square

III. THE INHOMOGENEOUS DOUBLE THINNING APPROACH

The approach that we propose for computing P_{cov} consists of introducing an equivalent abstraction for the system

model detailed in Section II-A that is based on I-PPPs. For ease of exposition, we first introduce the equivalent network model in general terms and then describe the IDT approach. The equivalent network model, in particular, is constituted by two I-PPPs, $\Phi_{\text{BS}}^{(F)}$ and $\Phi_{\text{BS}}^{(K)}$, which are constructed in a very special way and with the only purpose of approximating the original motion-invariant PP from the point of view of the typical user.

A. Cellular Networks Abstraction Modeling Based on I-PPPs

We consider the same system model as in Section II-A with a single exception: The BSs are modeled as the points of two *independent* isotropic I-PPPs, denoted by $\Phi_{\text{BS}}^{(F)}$ and $\Phi_{\text{BS}}^{(K)}$, with intensity measures $\Lambda_{\Phi_{\text{BS}}^{(F)}}(\cdot)$ and $\Lambda_{\Phi_{\text{BS}}^{(K)}}(\cdot)$, respectively. Since I-PPPs are non-stationary, the notion of typical user does not apply anymore. We are interested, on the other hand, in computing the coverage probability of a *probe* (or specific) MT that is located at the origin. The BS serving the probe MT is assumed to belong to $\Phi_{\text{BS}}^{(F)}$ and the interfering BSs are assumed to belong to $\Phi_{\text{BS}}^{(K)}$. More precisely, by considering the same cell association criterion as in Section II-C, the serving BS and the I-PPP, $\Phi_{\text{BS}}^{(I)}$, of interfering BSs can be formulated as follows:

$$\begin{aligned} x_0^{(F)} &= \arg \max_{x \in \Phi_{\text{BS}}^{(F)}} \{1/l(x)\} \\ \Phi_{\text{BS}}^{(I)} &= \Phi_{\text{BS}}^{(I)}(x_0^{(F)}) \\ &= \left\{x \in \Phi_{\text{BS}}^{(K)} : l(x) > L_0^{(F)} = l(x_0^{(F)})\right\} \end{aligned} \quad (5)$$

Remark 5: By construction, the I-PPPs $\Phi_{\text{BS}}^{(F)}$ and $\Phi_{\text{BS}}^{(K)}$ are independent. The I-PPPs $\Phi_{\text{BS}}^{(F)}$ and $\Phi_{\text{BS}}^{(I)}$ are, on the other hand, only *conditionally independent*, where the conditioning is meant upon the location of the serving BS, i.e., $x_0^{(F)}$. In (5), this conditioning accounts for the cell association criterion being used and is made explicit with the aid of the notation $\Phi_{\text{BS}}^{(I)} = \Phi_{\text{BS}}^{(I)}(x_0^{(F)})$. \square

In the proposed network model, which is based on I-PPPs whose serving and interfering BSs are defined in (5), the coverage probability of the probe MT at the origin can be formulated as:

$$\tilde{P}_{\text{cov}}^{(o)} = \Pr \left\{ \frac{P_{\text{tx}}g_0/L_0^{(F)}}{\sigma_N^2 + \sum_{x \in \Phi_{\text{BS}}^{(I)}} P_{\text{tx}}g_x/l(x)} > T \right\} \quad (6)$$

where the superscript (o) highlights that (6) holds for the probe MT at the origin.

The coverage probability, $\tilde{P}_{\text{cov}}^{(o)}$, in (6) is explicitly formulated in the following lemma.

Lemma 2: An analytical expression of the coverage probability in (6) is as follows:

$$\tilde{P}_{\text{cov}}^{(o)} = \int_0^{+\infty} \exp(-\xi T \sigma_N^2 / P_{\text{tx}}) \tilde{\mathcal{M}}_{L_0^{(F)}}(\xi; T) \tilde{f}_{L_0^{(F)}}(\xi) d\xi \quad (7)$$

where $\tilde{f}_{L_0^{(F)}}(\cdot)$ is the PDF of $L_0^{(F)}$ and $\tilde{\mathcal{M}}_{L_0^{(F)}}(\cdot; \cdot)$ is the Laplace functional of $\Phi_{BS}^{(I)}$ as follows:

$$\begin{aligned} \tilde{f}_{L_0^{(F)}}(\xi) &= \left(\frac{\xi}{\kappa}\right)^{1/\gamma} \frac{1}{\gamma\xi} \Lambda_{\Phi_{BS}^{(F)}}^{(1)} \left(\mathcal{B} \left(0, \left(\frac{\xi}{\kappa}\right)^{1/\gamma} \right) \right) \\ &\quad \times \exp \left(-\Lambda_{\Phi_{BS}^{(F)}} \left(\mathcal{B} \left(0, \left(\frac{\xi}{\kappa}\right)^{1/\gamma} \right) \right) \right) \\ \tilde{\mathcal{M}}_{L_0^{(F)}}(\xi; T) &= \exp \left(-\int_{\xi}^{+\infty} \left(1 + \frac{z}{T\xi}\right)^{-1} \left(\frac{z}{\kappa}\right)^{1/\gamma} \right. \\ &\quad \left. \times \frac{1}{\gamma z} \Lambda_{\Phi_{BS}^{(K)}}^{(1)} \left(\mathcal{B} \left(0, \left(\frac{z}{\kappa}\right)^{1/\gamma} \right) \right) dz \right) \quad (8) \end{aligned}$$

and $\Lambda_{(\cdot)}^{(1)}(\mathcal{B}(0, r)) = d\Lambda_{(\cdot)}(\mathcal{B}(0, r))/dr$ is the first-order derivative of the intensity measure.

Proof: It follows by using the same approach as in [9]. \square

The aim of the proposed IDT approach is to make the original network model based on the motion-invariant PP Ψ_{BS} and the equivalent network model based on the two conditionally independent I-PPPs $\Phi_{BS}^{(F)}$ and $\Phi_{BS}^{(I)}$ approximately the same from the coverage probability standpoint. In other words, the IDT approach aims to find two suitable intensity measures $\Lambda_{\Phi_{BS}^{(F)}}(\cdot)$ and $\Lambda_{\Phi_{BS}^{(K)}}(\cdot)$ such that $\tilde{P}_{cov}^{(o)} \approx P_{cov}$ holds for an arbitrary choice of the network parameters.

The intensity measures $\Lambda_{\Phi_{BS}^{(F)}}(\cdot)$ and $\Lambda_{\Phi_{BS}^{(K)}}(\cdot)$ are determined by taking into account five requirements: i) they need to depend only on the spatial characteristics of the original motion-invariant PP, which make them independent, e.g., of the transmission scheme and of the path-loss model being used, ii) they need to be determined by a few parameters and need to be simple to compute, iii) they need to lead to a tractable analytical expression of $\tilde{P}_{cov}^{(o)}$ as opposed to P_{cov} , iv) they need to lead to an analytical expression of the coverage that provides insight for system analysis and design, and v) they need to be applicable to advanced network models, e.g., that account for spatial blockages and multi-tier setups (see Sec. V). In the next two sections, we introduce the proposed intensity measures and the approach to obtain $\tilde{P}_{cov}^{(o)} \approx P_{cov}$.

B. IDT Approach: Proposed Intensity Measures of the I-PPPs

The intensity measure of an I-PPP is determined by the intensity function [32, Sec. 2.2]. Let $\lambda_{BS}^{(F)}(\cdot)$ and $\lambda_{BS}^{(K)}(\cdot)$ be the intensity functions of $\Phi_{BS}^{(F)}$ and $\Phi_{BS}^{(K)}$, respectively. Since the considered I-PPPs are isotropic, $\lambda_{BS}^{(F)}(\cdot)$ and $\lambda_{BS}^{(K)}(\cdot)$ are distance-dependent and angle-independent. The following holds:

$$\begin{aligned} \Lambda_{\Phi_{BS}^{(F)}}(\mathcal{B}(0, r)) &= 2\pi \int_0^r \lambda_{BS}^{(F)}(\zeta) \zeta d\zeta \\ \Lambda_{\Phi_{BS}^{(K)}}(\mathcal{B}(0, r)) &= 2\pi \int_0^r \lambda_{BS}^{(K)}(\zeta) \zeta d\zeta \quad (9) \end{aligned}$$

We propose different intensity functions for PPs that exhibit spatial inhibition and aggregation.

1) *Spatial Inhibition:* Let $(\check{a}_F, \check{b}_F, \check{c}_F)$ and $(\check{a}_K, \check{b}_K, \check{c}_K)$ be two triplets of non-negative real numbers such that $\check{c}_F \geq \check{b}_F \geq 1$ and $\check{b}_K \leq \check{c}_K \leq 1$. The following intensities are proposed:

$$\begin{aligned} \lambda_{BS}^{(F)}(r) &= \lambda_{BS} \check{c}_F \min \{ (\check{a}_F/\check{c}_F)r + \check{b}_F/\check{c}_F, 1 \} \\ \lambda_{BS}^{(K)}(r) &= \lambda_{BS} \min \{ \check{a}_K r + \check{b}_K, \check{c}_K \} \quad (10) \end{aligned}$$

2) *Spatial Aggregation:* Let $(\hat{a}_F, \hat{b}_F, \hat{c}_F)$ and $(\hat{a}_K, \hat{b}_K, \hat{c}_K)$ be two triplets of non-negative real numbers such that $\hat{c}_F \leq \hat{b}_F \leq 1$ and $\hat{b}_K \geq \hat{c}_K \geq 1$. The following intensities are proposed:

$$\begin{aligned} \lambda_{BS}^{(F)}(r) &= \lambda_{BS} \max \{ -\hat{a}_F r + \hat{b}_F, \hat{c}_F \} \\ \lambda_{BS}^{(K)}(r) &= \lambda_{BS} \hat{b}_K \max \{ -(\hat{a}_K/\hat{b}_K)r + 1, \hat{c}_K/\hat{b}_K \} \quad (11) \end{aligned}$$

Remark 6: Based on the definitions of the intensity functions in (10), the I-PPPs $\Phi_{BS}^{(F)}$ and $\Phi_{BS}^{(K)}$ can be obtained by first generating two H-PPPs with intensity functions $\lambda_{BS}\check{c}_F$ and λ_{BS} , respectively, and then independently thinning the points with retaining probabilities equal to $\min \{ (\check{a}_F/\check{c}_F)r + \check{b}_F/\check{c}_F, 1 \}$ and $\min \{ \check{a}_K r + \check{b}_K, \check{c}_K \}$, respectively. The constraints on the triplets of parameters $(\check{a}_F, \check{b}_F, \check{c}_F)$ and $(\check{a}_K, \check{b}_K, \check{c}_K)$ allows one to obtain a consistent thinning probability that is less than or equal to one. A similar comment holds for the definitions of the intensity functions in (11). \square

Remark 7: Besides simplicity and analytical tractability, the choice of $\min \{ \cdot, \cdot \}$ and $\max \{ \cdot, \cdot \}$ functions for the retaining probabilities in (10) and (11), respectively, has a profound rationale from the modeling standpoint. From the definition of $\min \{ \cdot, \cdot \}$ function, the BSs closer to the origin (where the probe MT is) are retained with a smaller probability. From the probe MT's standpoint, thus, the resulting I-PPP exhibits spatial repulsion. A similar line of thought applies to the $\max \{ \cdot, \cdot \}$ function, which allows one to model spatial clustering from the probe MT's standpoint, since the BSs closer to the origin are retained with a higher probability. \square

Remark 8: A network model based on H-PPPs is a special case of the model based on I-PPPs with intensity functions given in (10) and (11). Consider $a_F > 0$, $a_K > 0$, the H-PPP network model is obtained by setting $b_F = c_F = 1$ and $b_K = c_K = 1$ for PPs with repulsion or clustering. \square

For ease of writing, the intensity measures of PPs with spatial repulsion and clustering are denoted by $\Lambda_{\Phi_{BS}^{(\cdot)}}(\cdot; \check{a}_{(\cdot)}, \check{b}_{(\cdot)}, \check{c}_{(\cdot)}) = \check{\Lambda}_{\Phi_{BS}^{(\cdot)}}(\cdot)$ and $\Lambda_{\Phi_{BS}^{(\cdot)}}(\cdot; \hat{a}_{(\cdot)}, \hat{b}_{(\cdot)}, \hat{c}_{(\cdot)}) = \hat{\Lambda}_{\Phi_{BS}^{(\cdot)}}(\cdot)$, respectively.

The following lemma provides closed-form expressions for the intensity measures in (9).

Lemma 3: Let $\Upsilon(r; a, b, c)$ be defined as follows:

$$\begin{aligned} \Upsilon(r; a, b, c) &= 2\pi\lambda_{BS} \left((a/3)r^3 + (b/2)r^2 \right) \mathbb{1}(r \leq (c-b)/a) \\ &\quad + 2\pi\lambda_{BS} \left((c/2)r^2 - (c-b)^3/6a^2 \right) \mathbb{1}(r > (c-b)/a) \quad (12) \end{aligned}$$

The intensity measures in (10) can be formulated as $\check{\Lambda}_{\Phi_{\text{BS}}^{(\cdot)}}(\mathcal{B}(0, r)) = \Upsilon(r; \check{a}_{(\cdot)}, \check{b}_{(\cdot)}, \check{c}_{(\cdot)})$ and $\hat{\Lambda}_{\Phi_{\text{BS}}^{(\cdot)}}(\mathcal{B}(0, r)) = \Upsilon(r; -\hat{a}_{(\cdot)}, \hat{b}_{(\cdot)}, \hat{c}_{(\cdot)})$ for PPs that exhibit repulsion and clustering, respectively.

In addition, let $\Upsilon^{(1)}(r; a, b, c) = d\Upsilon(r; a, b, c)/dr$ be the first-order derivative of $\Upsilon(r; \cdot, \cdot, \cdot)$:

$$\begin{aligned} \Upsilon^{(1)}(r; a, b, c) &= 2\pi\lambda_{\text{BS}}(ar^2 + br) \mathbb{1}(r \leq (c-b)/a) \\ &\quad + 2\pi\lambda_{\text{BS}}cr \mathbb{1}(r > (c-b)/a) \end{aligned} \quad (13)$$

The first-order derivatives of the intensity measures are $\check{\Lambda}_{\Phi_{\text{BS}}^{(\cdot)}}^{(1)}(\mathcal{B}(0, r)) = \Upsilon^{(1)}(r; \check{a}_{(\cdot)}, \check{b}_{(\cdot)}, \check{c}_{(\cdot)})$ and $\hat{\Lambda}_{\Phi_{\text{BS}}^{(\cdot)}}^{(1)}(\mathcal{B}(0, r)) = \Upsilon^{(1)}(r; -\hat{a}_{(\cdot)}, \hat{b}_{(\cdot)}, \hat{c}_{(\cdot)})$ for PPs that exhibit repulsion and clustering, respectively.

Proof: It follows by inserting (10) and (11) in (9) and solving the integrals. \square

Remark 9: The functions $\Upsilon(r; \cdot, \cdot, \cdot)$ and $\Upsilon^{(1)}(r; \cdot, \cdot, \cdot)$ in (12) and (13) are continuous for $r \geq 0$ and for every triplet (a, b, c) . In particular, they are continuous if $r = (c-b)/a \geq 0$. \square

C. IDT Approach: Proposed Criterion for System Equivalence

From the intensity functions in (10) and (11), two triplets of parameters need to be estimated for approximating the network model based on a motion-invariant PP with the network model based on two conditionally independent I-PPPs. The aim of this section is to introduce a criterion for estimating these parameters in order to obtain $\tilde{P}_{\text{cov}}^{(o)} \approx P_{\text{cov}}$. By direct inspection of P_{cov} in (3) and $\tilde{P}_{\text{cov}}^{(o)}$ in (7), we evince that a sufficient condition for $\tilde{P}_{\text{cov}}^{(o)} \approx P_{\text{cov}}$ to hold is that the following two conditions are fulfilled simultaneously: $\tilde{f}_{L_0^{(F)}}(\xi) \approx f_{L_0}(\xi)$ and $\tilde{\mathcal{M}}_{I, L_0^{(F)}}(\xi; \mathbb{T}) \approx \mathcal{M}_{I, L_0}(\xi; \mathbb{T})$.

1) *Condition* $\tilde{f}_{L_0^{(F)}}(\xi) \approx f_{L_0}(\xi)$: $\tilde{f}_{L_0^{(F)}}(\cdot)$ and $f_{L_0}(\cdot)$ are the PDFs of the smallest path-loss of the typical MT (located at the origin without loss of generality) in the original network model and of the smallest path-loss of the probe MT at the origin in the equivalent network model based on I-PPPs. In the considered system model, the smallest path-loss is equivalent to the shortest distance. This assumption is not necessary for the application of the IDT approach, as better discussed in Section V. It helps, however, to introduce the essence of the proposed methodology. The PDF of the shortest distance of a PP to the origin is the first-order derivative of the CDD introduced in *Definition 1*. We evince that the condition $\tilde{f}_{L_0^{(F)}}(\xi) \approx f_{L_0}(\xi)$ is fulfilled if the CDD of the original motion-invariant PP and the CDD of the I-PPP $\Phi_{\text{BS}}^{(F)}$ are close to each other, i.e., $F_{\Psi_{\text{BS}}}(r) \approx F_{\Phi_{\text{BS}}^{(F)}}^{(o)}(r) = 1 - \exp\left(-\Lambda_{\Phi_{\text{BS}}^{(F)}}(\mathcal{B}(0, r))\right)$, where $\Lambda_{\Phi_{\text{BS}}^{(F)}}(\mathcal{B}(0, r)) = \check{\Lambda}_{\Phi_{\text{BS}}^{(F)}}(\mathcal{B}(0, r))$ and $\Lambda_{\Phi_{\text{BS}}^{(F)}}(\mathcal{B}(0, r)) = \hat{\Lambda}_{\Phi_{\text{BS}}^{(F)}}(\mathcal{B}(0, r))$ if Ψ_{BS} exhibits spatial repulsion and clustering, respectively.

2) *Condition* $\tilde{\mathcal{M}}_{I, L_0^{(F)}}(\xi; \mathbb{T}) \approx \mathcal{M}_{I, L_0}(\xi; \mathbb{T})$: $\mathcal{M}_{I, L_0^{(F)}}(\cdot; \cdot)$ and $\mathcal{M}_{I, L_0}(\cdot; \cdot)$ are the Laplace functionals of the PPs of interfering BSs $\Psi_{\text{BS}}^{(I)}$ and $\Phi_{\text{BS}}^{(I)}$ defined in (5), respectively.

From (8), $\tilde{\mathcal{M}}_{I, L_0^{(F)}}(\cdot; \cdot)$ depends uniquely on the intensity measure of the I-PPP $\Phi_{\text{BS}}^{(K)}$, i.e., $\Lambda_{\Phi_{\text{BS}}^{(K)}}(\cdot)$. From (4), the computation of $\mathcal{M}_{I, L_0}(\cdot; \cdot)$ necessitates the reduced Palm distribution of the motion-invariant PP Ψ_{BS} . Since the latter distribution may not be either known or tractable, our approach for fulfilling the condition $\tilde{\mathcal{M}}_{I, L_0^{(F)}}(\xi; \mathbb{T}) \approx \mathcal{M}_{I, L_0}(\xi; \mathbb{T})$ is based on a second-order moment approximation of the spatial interactions among the points of the motion-invariant PP Ψ_{BS} [30, Sec. 7.3]. More precisely, our approach relies on *Remark 3* and *Definition 2*. From *Remark 3*, we know that the intensity measure of an I-PPP coincides with its non-regularized K-function. As a result, we propose to choose the intensity measure of $\Phi_{\text{BS}}^{(K)}$ such that it coincides with the non-regularized K-function of Ψ_{BS} , i.e., $\Lambda_{\Phi_{\text{BS}}^{(K)}}(\mathcal{B}(0, r)) \approx K_{\Psi_{\text{BS}}}(r)$, where $\Lambda_{\Phi_{\text{BS}}^{(K)}}(\mathcal{B}(0, r)) = \check{\Lambda}_{\Phi_{\text{BS}}^{(K)}}(\mathcal{B}(0, r))$ and $\Lambda_{\Phi_{\text{BS}}^{(K)}}(\mathcal{B}(0, r)) = \hat{\Lambda}_{\Phi_{\text{BS}}^{(K)}}(\mathcal{B}(0, r))$ if Ψ_{BS} exhibits spatial repulsion and clustering, respectively. By using this approach, we ensure that the average number of interfering BSs viewed by the typical MT of the original network model is the same as the average number of interfering BSs viewed by the probe MT at the origin of the equivalent network model based on I-PPPs.

Remark 10: The non-regularized K-Function of motion-invariant PPs provides, by definition, the average number of BSs viewed by a BS of the PP (whose contribution is ignored) within a ball centered at the BS and of fixed radius. There is no ambiguity, however, in saying that the non-regularized K-Function yields the average number of interfering BSs viewed by the typical MT. This originates from the properties of motion-invariant PPs as detailed in [20, Sec. III]. In simple terms, the BSs of a motion-invariant PP can be translated, without altering the statistics of the PP, so that the location of the serving BS is moved to the location of the typical MT. \square

Remark 11: Why is the equivalent network model based on two I-PPPs? Isn't one I-PPP sufficient? The reason why the IDT approach is based on two I-PPPs can be understood from the approximations proposed to obtain the intensity measures of the I-PPPs. The intensity measures of $\Phi_{\text{BS}}^{(F)}$ and $\Phi_{\text{BS}}^{(K)}$ are obtained from the F-function and non-regularized K-function of the motion-invariant PP Ψ_{BS} . Based on, e.g., [20, eqs. (10) and (19)] and [23], we observe that the F-function and non-regularized K-function of repulsive PPs have opposite trends compared with the same functions of a H-PPP: The F-function of a repulsive PP is usually greater than the F-function of a H-PPP, while the K-function of a repulsive PP is usually smaller than the K-function of a H-PPP. These conflicting trends, which determine the distribution of the distances of serving and interfering BSs, are difficult to model with a single I-PPP. \square

Remark 12: In network models where the smallest path-loss is equivalent to the shortest distance, the proposed equivalent network model may be obtained by using only the I-PPP obtained from the non-regularized K-function. The serving BS may, in fact, be obtained by generating a single point (rather than the complete I-PPP based on the F-function), whose distance from the probe MT is a random variable with distribution

TABLE II

F-FUNCTION AND K-FUNCTION OF PPS. EMPIRICAL (EMP.) MEANS THAT NO CLOSED-FORM IS AVAILABLE AND THAT THE FUNCTIONS ARE OBTAINED FROM STATISTICAL DATA GENERATED BY USING R [30]

PP	F-Function	K-Function
DPP	[23]	[41]
GPP	[20]	[20]
Lattice PP	[28], [42]	[28], [42]
LGCP	[43]	[44, p. 745]
PHP	Emp. [30, Sec. 8.3]	Emp. [30, Sec. 7.3]
MCPP	Emp. [45]	Emp. [30, p. 818]

equal to the F-function. In general, however, the generation of a complete I-PPP may be still more convenient due to its simplicity of implementation and generality. In network models where the smallest path-loss is not equivalent to the shortest distance, both I-PPPs are needed in order to account for the distance and the path-loss model and, hence, to correctly identify the serving BS. An example is the network model in the presence of spatial blockages that is analyzed in Section V-A. \square

Remark 13: The proposed approximations based on the F-function and non-regularized K-function are convenient for two reasons: i) they can be readily estimated from empirical data sets or by using open-source statistical toolboxes for analyzing PPs [30]³ and ii) they are available in closed-form for many PPs that exhibit spatial inhibition and aggregation. As far as the PPs of interest for this paper are concerned, Table II summarizes where they can be found. \square

In summary, the triplets of parameters that determine the intensity measures $\Lambda_{\Phi_{\text{BS}}^{(F)}}(\cdot)$ and $\Lambda_{\Phi_{\text{BS}}^{(K)}}(\cdot)$ in *Lemma 3* can be obtained by solving the minimization problems in (14) shown at the bottom of the next page, where the definitions $\Omega_F = \{(\check{a}_F, \check{b}_F, \check{c}_F) : \check{c}_F \geq \check{b}_F \geq 1\}$ and $\Omega_K = \{(\check{a}_K, \check{b}_K, \check{c}_K) : \check{b}_K \leq \check{c}_K \leq 1\}$ or $\Omega_F = \{(\hat{a}_F, \hat{b}_F, \hat{c}_F) : \hat{c}_F \leq \hat{b}_F \leq 1\}$ and $\Omega_K = \{(\hat{a}_K, \hat{b}_K, \hat{c}_K) : \hat{b}_K \geq \hat{c}_K \geq 1\}$ hold if the motion-invariant

PP Ψ_{BS} exhibits spatial repulsion or clustering, respectively.

Remark 14: The non-linear optimization problem in (14) aims to minimize the error between the exact (or empirically estimated) F-function and non-regularized K-function of Ψ_{BS} and the corresponding functions of $\Phi_{\text{BS}}^{(F)}$ and $\Phi_{\text{BS}}^{(K)}$, respectively. The errors are, in general, computed over the entire positive real axis, i.e., for $r \geq 0$. If $F_{\Psi_{\text{BS}}}(\cdot)$ and $K_{\Psi_{\text{BS}}}(\cdot)$ are estimated from empirical data, on the other hand, the errors are computed for $0 \leq r \leq R_A$, where R_A is the largest distance from the origin of the geographical region of interest, i.e., the network radius (some examples are available in Table VI). Equation (14) can be efficiently solved by employing the function `lsqcurvefit` that is available Matlab. Further details are provided in Section VI. \square

³Similar to [1], the density of BSs, λ_{BS} , needs to be estimated from the data set, e.g., as described in [30, Sec. 6.2].

IV. TRACTABLE ANALYTICAL FRAMEWORK OF THE COVERAGE PROBABILITY

With the aid of the IDT approach, we introduce a new tractable expression of the coverage probability for cellular networks whose BSs exhibit spatial inhibition and aggregation. Based on *Lemma 3*, the analysis of network models with spatial repulsion and clustering is unified by considering a generic triplet of parameters $(a_{(\cdot)}, b_{(\cdot)}, c_{(\cdot)})$ and by setting $(a_{(\cdot)}, b_{(\cdot)}, c_{(\cdot)}) = (\check{a}_{(\cdot)}, \check{b}_{(\cdot)}, \check{c}_{(\cdot)})$ and $(a_{(\cdot)}, b_{(\cdot)}, c_{(\cdot)}) = (-\hat{a}_{(\cdot)}, \hat{b}_{(\cdot)}, \hat{c}_{(\cdot)})$ for PPs that exhibit spatial inhibition and aggregation, respectively.

The following theorem provides a tractable expression for $\tilde{P}_{\text{cov}}^{(\circ)}$ in (6). Two case studies are considered: i) the network is infinitely large and ii) the network has a finite size whose radius is R_A . The second case study is useful for comparing the analytical frameworks against estimates obtained by using empirical data, especially for small values of the path-loss exponent. This is because it is not possible, in many cases, to obtain or generate data sets for very large geographical regions.

Theorem 1: Based on the intensity measures in (9)-(11), $\tilde{P}_{\text{cov}}^{(\circ)}$ in (6) can be formulated as in (15) shown at the bottom of the next page, where $\Theta \rightarrow \infty$ and $\mathcal{I}(\xi) = \mathcal{I}_{\infty}(\xi)$ for infinite-size networks, $\Theta \rightarrow \kappa R_A^\gamma$ and $\mathcal{I}(\xi) = \mathcal{I}_{R_A}(\xi)$ for finite-size networks of radius R_A , and $\mathcal{I}_{\infty}(\cdot)$, $\mathcal{I}_{R_A}(\cdot)$, $\mathcal{U}_{\text{IN}}(\cdot)$, $\mathcal{U}_{\text{OUT}}(\cdot)$ are defined in Table III.

Proof: See Appendix A. \square

Remark 15: From *Remark 8*, the coverage probability of H-PPPs follows from (15) by setting $b_F = c_F = 1$ and $b_K = c_K = 1$. Throughout this paper, it is denoted by $P_{\text{cov}}^{(\text{H-PPP})}$. \square

Remark 16: The coverage probability in (15) is formulated in terms of a single integral whose numerical complexity is not higher than that of currently available frameworks based on H-PPPs [1]. Since (15) cannot be explicitly computed, a promising research direction is to develop closed-form bounds and approximations for $\tilde{P}_{\text{cov}}^{(\circ)}$ in order to simplify analysis and optimization. \square

A. Comparison With Homogeneous Poisson Point Processes

From *Remark 8*, it follows that network models based on H-PPPs constitute a special case of network models based on I-PPPs, i.e., the IDT approach. In this section, we are interested in comparing the coverage of PPs that exhibit spatial inhibition and aggregation against the coverage of H-PPPs. More precisely, we aim to identify sufficient conditions on the triplets of parameters (a_F, b_F, c_F) and (a_K, b_K, c_K) that make the coverage probability of cellular networks with spatial repulsion and clustering better and worse than the coverage probability of H-PPPs, respectively. The main result is reported in *Proposition 1*. Three lemmas used for its proof are provided as follows.

Lemma 4: The intensity measure of a H-PPP with constant intensity function λ_{BS} is $\Lambda_{\text{H-PPP}}(\mathcal{B}(0, r)) = \pi \lambda_{\text{BS}} r^2$ and its first-order derivative is $\Lambda_{\text{H-PPP}}^{(1)}(\mathcal{B}(0, r)) = 2\pi \lambda_{\text{BS}} r$.

Proof: It follows from *Remark 8* and *Lemma 3*. \square

Lemma 5: Let Ψ_{BS} be a motion-invariant PP with spatial repulsion. Let $\Lambda_{\Phi_{\text{BS}}^{(F)}}(\mathcal{B}(0, r); \check{a}_F, \check{b}_F, \check{c}_F)$ and

TABLE III
AUXILIARY FUNCTIONS USED IN *Theorem 1*

Function Definition
$\mathcal{U}_{\text{IN}}(\xi) = 2\pi\lambda_{\text{BS}} \left(\frac{a_{\text{F}}}{\gamma\xi} \left(\frac{\xi}{\kappa} \right)^{3/\gamma} + \frac{b_{\text{F}}}{\gamma\xi} \left(\frac{\xi}{\kappa} \right)^{2/\gamma} \right) \exp \left(-2\pi\lambda_{\text{BS}} \left(\frac{a_{\text{F}}}{3} \left(\frac{\xi}{\kappa} \right)^{3/\gamma} + \frac{b_{\text{F}}}{2} \left(\frac{\xi}{\kappa} \right)^{2/\gamma} \right) \right)$
$\mathcal{U}_{\text{OUT}}(\xi) = 2\pi\lambda_{\text{BS}} \frac{c_{\text{F}}}{\gamma\xi} \left(\frac{\xi}{\kappa} \right)^{2/\gamma} \exp \left(-2\pi\lambda_{\text{BS}} \left(\frac{c_{\text{F}}}{2} \left(\frac{\xi}{\kappa} \right)^{2/\gamma} - \frac{(c_{\text{F}} - b_{\text{F}})^3}{6a_{\text{F}}^2} \right) \right)$
$\mathcal{I}_1(\xi) = 2\pi\lambda_{\text{BS}} \frac{a_{\text{K}}}{3} \left(\frac{c_{\text{K}} - b_{\text{K}}}{a_{\text{K}}} \right)^3 {}_2F_1 \left(1, \frac{3}{\gamma}, 1 + \frac{3}{\gamma}, -\frac{\kappa}{T\xi} \left(\frac{c_{\text{K}} - b_{\text{K}}}{a_{\text{K}}} \right)^\gamma \right) \mathbb{1} \left(\xi \leq \kappa \left(\frac{c_{\text{K}} - b_{\text{K}}}{a_{\text{K}}} \right)^\gamma \right)$
$\mathcal{I}_2(\xi) = 2\pi\lambda_{\text{BS}} \frac{b_{\text{K}}}{2} \left(\frac{c_{\text{K}} - b_{\text{K}}}{a_{\text{K}}} \right)^2 {}_2F_1 \left(1, \frac{2}{\gamma}, 1 + \frac{2}{\gamma}, -\frac{\kappa}{T\xi} \left(\frac{c_{\text{K}} - b_{\text{K}}}{a_{\text{K}}} \right)^\gamma \right) \mathbb{1} \left(\xi \leq \kappa \left(\frac{c_{\text{K}} - b_{\text{K}}}{a_{\text{K}}} \right)^\gamma \right)$
$\mathcal{I}_3(\xi) = -2\pi\lambda_{\text{BS}} \frac{a_{\text{K}}}{3} \left(\frac{\xi}{\kappa} \right)^{3/\gamma} {}_2F_1 \left(1, \frac{3}{\gamma}, 1 + \frac{3}{\gamma}, -\frac{1}{T} \right) \mathbb{1} \left(\xi \leq \kappa \left(\frac{c_{\text{K}} - b_{\text{K}}}{a_{\text{K}}} \right)^\gamma \right)$
$\mathcal{I}_4(\xi) = -2\pi\lambda_{\text{BS}} \frac{b_{\text{K}}}{2} \left(\frac{\xi}{\kappa} \right)^{2/\gamma} {}_2F_1 \left(1, \frac{2}{\gamma}, 1 + \frac{2}{\gamma}, -\frac{1}{T} \right) \mathbb{1} \left(\xi \leq \kappa \left(\frac{c_{\text{K}} - b_{\text{K}}}{a_{\text{K}}} \right)^\gamma \right)$
$\mathcal{I}_5(\xi) = -2\pi\lambda_{\text{BS}} \frac{c_{\text{K}}}{2} \left(\frac{c_{\text{K}} - b_{\text{K}}}{a_{\text{K}}} \right)^2 \left(1 - {}_2F_1 \left(1, -\frac{2}{\gamma}, 1 - \frac{2}{\gamma}, -\frac{T\xi}{\kappa} \left(\frac{c_{\text{K}} - b_{\text{K}}}{a_{\text{K}}} \right)^{-\gamma} \right) \right) \mathbb{1} \left(\xi \leq \kappa \left(\frac{c_{\text{K}} - b_{\text{K}}}{a_{\text{K}}} \right)^\gamma \right)$
$\mathcal{I}_6(\xi) = -2\pi\lambda_{\text{BS}} \frac{c_{\text{K}}}{2} \left(\frac{\xi}{\kappa} \right)^{2/\gamma} \left(1 - {}_2F_1 \left(1, -\frac{2}{\gamma}, 1 - \frac{2}{\gamma}, -T \right) \right) \mathbb{1} \left(\xi \geq \kappa \left(\frac{c_{\text{K}} - b_{\text{K}}}{a_{\text{K}}} \right)^\gamma \right)$
$\mathcal{I}_7(\xi) = 2\pi\lambda_{\text{BS}} \frac{c_{\text{K}}}{2} R_{\text{A}}^2 {}_2F_1 \left(1, \frac{2}{\gamma}, 1 + \frac{2}{\gamma}, -\frac{\kappa}{T\xi} R_{\text{A}}^\gamma \right) \mathbb{1} \left(\xi \leq \kappa \left(\frac{c_{\text{K}} - b_{\text{K}}}{a_{\text{K}}} \right)^\gamma \right)$
$\mathcal{I}_8(\xi) = -2\pi\lambda_{\text{BS}} \frac{c_{\text{K}}}{2} \left(\frac{c_{\text{K}} - b_{\text{K}}}{a_{\text{K}}} \right)^2 {}_2F_1 \left(1, \frac{2}{\gamma}, 1 + \frac{2}{\gamma}, -\frac{\kappa}{T\xi} \left(\frac{c_{\text{K}} - b_{\text{K}}}{a_{\text{K}}} \right)^\gamma \right) \mathbb{1} \left(\xi \leq \kappa \left(\frac{c_{\text{K}} - b_{\text{K}}}{a_{\text{K}}} \right)^\gamma \right)$
$\mathcal{I}_9(\xi) = 2\pi\lambda_{\text{BS}} \frac{c_{\text{K}}}{2} R_{\text{A}}^2 {}_2F_1 \left(1, \frac{2}{\gamma}, 1 + \frac{2}{\gamma}, -\frac{\kappa}{T\xi} R_{\text{A}}^\gamma \right) \mathbb{1} \left(\xi \geq \kappa \left(\frac{c_{\text{K}} - b_{\text{K}}}{a_{\text{K}}} \right)^\gamma \right)$
$\mathcal{I}_{10}(\xi) = -2\pi\lambda_{\text{BS}} \frac{c_{\text{K}}}{2} \left(\frac{\xi}{\kappa} \right)^{2/\gamma} {}_2F_1 \left(1, \frac{2}{\gamma}, 1 + \frac{2}{\gamma}, -\frac{1}{T} \right) \mathbb{1} \left(\xi \geq \kappa \left(\frac{c_{\text{K}} - b_{\text{K}}}{a_{\text{K}}} \right)^\gamma \right)$
$\mathcal{I}_\infty(\xi) = \mathcal{I}_1(\xi) + \mathcal{I}_2(\xi) + \mathcal{I}_3(\xi) + \mathcal{I}_4(\xi) + \mathcal{I}_5(\xi) + \mathcal{I}_6(\xi)$
$\mathcal{I}_{\text{R}_\text{A}}(\xi) = \mathcal{I}_1(\xi) + \mathcal{I}_2(\xi) + \mathcal{I}_3(\xi) + \mathcal{I}_4(\xi) + \mathcal{I}_7(\xi) + \mathcal{I}_8(\xi) + \mathcal{I}_9(\xi) + \mathcal{I}_{10}(\xi)$

$\Lambda_{\Phi_{\text{BS}}^{(\kappa)}}(\mathcal{B}(0, r); \check{a}_{\text{K}}, \check{b}_{\text{K}}, \check{c}_{\text{K}})$ be the intensity measures of the equivalent I-PPPs $\Phi_{\text{BS}}^{(F)}$ and $\Phi_{\text{BS}}^{(K)}$ obtained by applying the IDT approach in (14). If $\check{c}_{\text{F}} \geq b_{\text{F}} \geq 1$ and $\check{b}_{\text{K}} \leq \check{c}_{\text{K}} \leq 1$, then:

$$\begin{aligned} \check{\Lambda}_{\Phi_{\text{BS}}^{(F)}}(\mathcal{B}(0, r)) &\geq \Lambda_{\text{H-PPP}}(\mathcal{B}(0, r)) \\ \check{\Lambda}_{\Phi_{\text{BS}}^{(F)}}^{(1)}(\mathcal{B}(0, r)) &\geq \Lambda_{\text{H-PPP}}^{(1)}(\mathcal{B}(0, r)) \\ \check{\Lambda}_{\Phi_{\text{BS}}^{(K)}}(\mathcal{B}(0, r)) &\leq \Lambda_{\text{H-PPP}}(\mathcal{B}(0, r)) \\ \check{\Lambda}_{\Phi_{\text{BS}}^{(K)}}^{(1)}(\mathcal{B}(0, r)) &\leq \Lambda_{\text{H-PPP}}^{(1)}(\mathcal{B}(0, r)) \end{aligned} \quad (16)$$

Proof: It follows by direct inspection of $\varepsilon(r) = \Lambda_{\Phi_{\text{BS}}^{(\cdot)}}(\mathcal{B}(0, r); \check{a}_{(\cdot)}, \check{b}_{(\cdot)}, \check{c}_{(\cdot)}) - \Lambda_{\text{H-PPP}}(\mathcal{B}(0, r))$ and of its first-order derivative computed with respect to r . \square

Lemma 6: Let Ψ_{BS} be a motion-invariant PP with spatial clustering. Let $\Lambda_{\Phi_{\text{BS}}^{(F)}}(\mathcal{B}(0, r); \hat{a}_{\text{F}}, \hat{b}_{\text{F}}, \hat{c}_{\text{F}})$ and $\Lambda_{\Phi_{\text{BS}}^{(K)}}(\mathcal{B}(0, r); \hat{a}_{\text{K}}, \hat{b}_{\text{K}}, \hat{c}_{\text{K}})$ be the intensity measures of the equivalent I-PPPs $\Phi_{\text{BS}}^{(F)}$ and $\Phi_{\text{BS}}^{(K)}$ obtained by applying the IDT approach in (14). If $\hat{c}_{\text{F}} \leq \hat{b}_{\text{F}} \leq 1$ and $\hat{b}_{\text{K}} \geq \hat{c}_{\text{K}} \geq 1$, then:

$$\begin{aligned} \hat{\Lambda}_{\Phi_{\text{BS}}^{(F)}}(\mathcal{B}(0, r)) &\leq \Lambda_{\text{H-PPP}}(\mathcal{B}(0, r)) \\ \hat{\Lambda}_{\Phi_{\text{BS}}^{(F)}}^{(1)}(\mathcal{B}(0, r)) &\leq \Lambda_{\text{H-PPP}}^{(1)}(\mathcal{B}(0, r)) \\ \hat{\Lambda}_{\Phi_{\text{BS}}^{(K)}}(\mathcal{B}(0, r)) &\geq \Lambda_{\text{H-PPP}}(\mathcal{B}(0, r)) \\ \hat{\Lambda}_{\Phi_{\text{BS}}^{(K)}}^{(1)}(\mathcal{B}(0, r)) &\geq \Lambda_{\text{H-PPP}}^{(1)}(\mathcal{B}(0, r)) \end{aligned} \quad (17)$$

Proof: It follows similar to the proof of *Lemma 5*. \square

$$\begin{aligned} (a_{\text{F}}, b_{\text{F}}, c_{\text{F}}) &= \arg \min_{(a, b, c) \in \Omega_{\text{F}}} \left\{ \int_0^{+\infty} \left[F_{\Psi_{\text{BS}}}(r) - \left(1 - \exp \left(-\Lambda_{\Phi_{\text{BS}}^{(F)}}(\mathcal{B}(0, r); a, b, c) \right) \right) \right]^2 dr \right\} \\ (a_{\text{K}}, b_{\text{K}}, c_{\text{K}}) &= \arg \min_{(a, b, c) \in \Omega_{\text{K}}} \left\{ \int_0^{+\infty} \left[K_{\Psi_{\text{BS}}}(r) - \Lambda_{\Phi_{\text{BS}}^{(K)}}(\mathcal{B}(0, r); a, b, c) \right]^2 dr \right\} \end{aligned} \quad (14)$$

$$\begin{aligned} \tilde{\text{P}}_{\text{cov}}^{(\circ)} &= \int_0^{\kappa((c_{\text{F}} - b_{\text{F}})/a_{\text{F}})^\gamma} \exp(-\xi T \sigma_{\text{N}}^2 / P_{\text{tx}}) \exp(-\mathcal{I}(\xi)) \mathcal{U}_{\text{IN}}(\xi) d\xi \\ &\quad + \int_{\kappa((c_{\text{F}} - b_{\text{F}})/a_{\text{F}})^\gamma}^{\Theta} \exp(-\xi T \sigma_{\text{N}}^2 / P_{\text{tx}}) \exp(-\mathcal{I}(\xi)) \mathcal{U}_{\text{OUT}}(\xi) d\xi \end{aligned} \quad (15)$$

$$1/\mathcal{G}_\infty = \pi\lambda_{\text{BS}} \int_0^{(\check{c}_K - \check{b}_K)/\check{a}_K} \left(\frac{x^\gamma (\check{c}_K - \check{b}_K)^{3-\gamma}}{\gamma-3 \check{a}_K^{2-\gamma}} + \frac{\gamma-2}{\gamma-3} \check{a}_K x^3 + \check{b}_K x^2 \right) \varpi_F(x) dx + \pi\lambda_{\text{BS}} \check{c}_K \int_{(\check{c}_K - \check{b}_K)/\check{a}_K}^{+\infty} x^2 \varpi_F(x) dx \quad (19)$$

Remark 17: The findings reported in *Lemma 5* and *Lemma 6* provide relevant insight and intuition on the impact of spatial repulsion and clustering among the BSs of cellular networks. In the presence of spatial repulsion, *Lemma 5* states that, under some assumptions on the parameters, the CDD of I-PPPs is greater than the CDD of H-PPPs. This follows from *Definition 1* and the condition $\check{\Lambda}_{\Phi_{\text{BS}}^{(F)}}(\cdot) \geq \Lambda_{\text{H-PPP}}(\cdot)$. In addition, *Lemma 5* states that the average number of interfering BSs viewed by the typical MT in the presence of spatial repulsion is smaller than the average number of interferers in network models with complete spatial randomness (i.e., based on H-PPPs). This follows from *Definition 2* and the condition $\check{\Lambda}_{\Phi_{\text{BS}}^{(K)}}(\cdot) \leq \Lambda_{\text{H-PPP}}(\cdot)$. Compared with H-PPPs, in other words, network models based on PPs with spatial repulsion result, from the standpoint of the typical MT, in the serving BS being closer to the typical MT and in a smaller number, on average, of interfering BSs around it. This is consistent with *Remark 11* and confirms a *hidden intuition* on the impact of spatial repulsion in cellular networks. *Lemma 6*, on the other hand, provides opposite conclusions about the impact of spatial clustering: Compared with H-PPPs, the serving BS is more distant from the typical MT and the average number of interferers around it is larger. In Section VI, we show that the conditions on the parameters stated in *Lemma 5* and *Lemma 6* hold for several empirical cellular network deployments available in the literature. \square

Proposition 1: Let $\tilde{P}_{\text{cov}}^{(\circ)}$ be the coverage probability in *Theorem 1* and $P_{\text{cov}}^{(\text{H-PPP})}$ be the coverage probability of a H-PPP according to *Remark 15*. Then, $\tilde{P}_{\text{cov}}^{(\circ)} \geq P_{\text{cov}}^{(\text{H-PPP})}$ under the assumptions of *Lemma 5* and $\tilde{P}_{\text{cov}}^{(\circ)} \leq P_{\text{cov}}^{(\text{H-PPP})}$ under the assumptions of *Lemma 6*. \square

Proof: See Appendix B. \square

Remark 18: *Proposition 1* yields the conditions that need to be fulfilled by an I-PPP to be stochastically greater or smaller than a H-PPP according to the coverage probability order [40]. Appendix B, in particular, provides a formal proof of the stochastic ordering that exists between I-PPPs and H-PPPs, as a function of the triplet of parameters $(\check{a}_F, \check{b}_F, \check{c}_F)$ and $(\check{a}_K, \check{b}_K, \check{c}_K)$. \square

B. AS-A-PPP: Simplified Expression of the Deployment Gain

In [18] and [19], the author introduces the ASAPP approach, which consists of obtaining the coverage probability of repulsive PPs through a right-shift of the coverage probability under the H-PPP model. The right-shift to apply is termed asymptotic deployment gain. In this section, we show that the asymptotic deployment gain of the network model based on I-PPPs has a simple analytical formulation. For simplicity, we focus our attention on the original

definition of the asymptotic deployment gain, henceforth denoted by \mathcal{G}_∞ , for interference-limited cellular networks, i.e., for $\sigma_N^2 = 0$. From [18, eq. (5)], \mathcal{G}_∞ can be formulated as $\mathcal{G}_\infty = (\text{MISR}_{\text{IDT}}/\text{MISR}_{\text{H-PPP}})^{-1}$, where MISR stands for Mean Interference-to-Signal Ratio, $\text{MISR}_{\text{H-PPP}} = 2/(\gamma - 2)$ for H-PPPs and the following holds for I-PPPs with spatial repulsion:

$$\text{MISR}_{\text{IDT}} = \int_0^{+\infty} x^\gamma \left(\int_x^{+\infty} y^{-\gamma} \check{\Lambda}_{\Phi_{\text{BS}}^{(K)}}^{(1)}(\mathcal{B}(0, y)) dy \right) \times \check{\Lambda}_{\Phi_{\text{BS}}^{(F)}}^{(1)}(\mathcal{B}(0, x)) \exp\left(-\check{\Lambda}_{\Phi_{\text{BS}}^{(F)}}(\mathcal{B}(0, x))\right) dx \quad (18)$$

The following proposition provides us with a tractable expression of \mathcal{G}_∞ based on (18).

Proposition 2: The asymptotic deployment gain \mathcal{G}_∞ can be formulated as in (19) shown at the top of this page, where $\varpi_F(x) = \check{\Lambda}_{\Phi_{\text{BS}}^{(F)}}^{(1)}(\mathcal{B}(0, x)) \exp\left(-\check{\Lambda}_{\Phi_{\text{BS}}^{(F)}}(\mathcal{B}(0, x))\right)$.

Proof: It follows by inserting (12) and (13) in (18), and by computing the inner integral. \square

Remark 19: The analytical expression of \mathcal{G}_∞ in (19) holds for $\gamma \neq 3$. The setup $\gamma = 3$ can be obtained from (18) as a special case. For brevity, the final formula is not reported in the present paper. \square

The asymptotic deployment gain in (19) may be further simplified and studied as a function of the triplets $(\check{a}_F, \check{b}_F, \check{c}_F)$ and $(\check{a}_K, \check{b}_K, \check{c}_K)$. This is, however, beyond the scope of the present paper. Our aim is to show an important application of the proposed IDT approach for modeling cellular networks: The simple calculation of \mathcal{G}_∞ under the proposed modeling approach, as opposed to the general definition based on the Palm measure [25]. The generalization of (19) to multi-tier and other network models can be obtained by applying the methods discussed in Section V.

V. GENERALIZATIONS

In this section, we generalize the IDT approach for application to system models that account for spatial blockages and multi-tier network deployments. Due to space limitations, we focus our attention only on the computation of the coverage probability. It can be shown, however, that the findings in *Lemma 5*, *Lemma 6*, and *Proposition 1* apply unaltered to the system model with spatial blockages. The proofs follow the same rationale as the methods reported in Section IV-A.

A. Cellular Networks in the Presence of Spatial Blockages

Due to its mathematical tractability yet accuracy for modeling spatial blockages, we adopt the distance-dependent

TABLE IV
AUXILIARY FUNCTIONS USED IN *Theorem 2* ($D_F = (c_F - b_F)/a_F$ AND $D_K = (c_K - b_K)/a_K$)

Function Definition ($\mathcal{J}_1(\cdot)$ and $\mathcal{J}_2(\cdot)$ are defined in Appendix A)
$\mathcal{U}_0(\xi) = 2\pi\lambda_{BS} \sum_{s \in \{\text{los}, \text{nlos}\}} (\gamma_s \xi)^{-1} (\xi/\kappa_s)^{1/\gamma_s} \phi_s \left((\xi/\kappa_s)^{1/\gamma_s} \right) \exp \left(-2\pi\lambda_{BS} \sum_{s \in \{\text{los}, \text{nlos}\}} \varphi_s \left((\xi/\kappa_s)^{1/\gamma_s} \right) \right)$
$\phi_s(\zeta) = \phi_{s,1}(\zeta) \mathbb{1}(\zeta \leq \min\{D_F, D_B\}) + \phi_{s,2}(\zeta) \mathbb{1}(D_B \leq \zeta \leq D_F, D_B \leq D_F)$ $+ \phi_{s,3}(\zeta) \mathbb{1}(D_F \leq \zeta \leq D_B, D_F \leq D_B) + \phi_{s,4}(\zeta) \mathbb{1}(\zeta \geq D_F, D_B \leq D_F) + \phi_{s,5}(\zeta) \mathbb{1}(\zeta \geq D_B, D_F \leq D_B)$
$\varphi_s(\zeta) = \varphi_{s,1}(\zeta) \mathbb{1}(\zeta \leq \min\{D_F, D_B\}) + \varphi_{s,2}(\zeta) \mathbb{1}(D_B \leq \zeta \leq D_F, D_B \leq D_F)$ $+ \varphi_{s,3}(\zeta) \mathbb{1}(D_F \leq \zeta \leq D_B, D_F \leq D_B) + \varphi_{s,4}(\zeta) \mathbb{1}(\zeta \geq D_F, D_B \leq D_F) + \varphi_{s,5}(\zeta) \mathbb{1}(\zeta \geq D_B, D_F \leq D_B)$
$\varphi_{s,1}(\zeta) = q_s^{(\text{in})} (a_F (\zeta^3/3) + b_F (\zeta^2/2)), \quad \varphi_{s,3}(\zeta) = q_s^{(\text{in})} (-a_F (D_F^3/6) + c_F (\zeta^2/2))$ $\varphi_{s,2}(\zeta) = q_s^{(\text{out})} (a_F (\zeta^3/3) + b_F (\zeta^2/2)) + (q_s^{(\text{in})} - q_s^{(\text{out})}) (a_F (D_B^3/3) + b_F (D_B^2/2))$
$\varphi_{s,4}(\zeta) = q_s^{(\text{in})} (a_F (D_B^3/3) + b_F (D_B^2/2)) - q_s^{(\text{out})} a_F ((D_F^3/6) + (D_B^3/3)) + q_s^{(\text{out})} (c_F (\zeta^2/2) - b_F (D_B^2/2))$ $\varphi_{s,5}(\zeta) = q_s^{(\text{in})} (-a_F (D_F^3/6) + c_F (D_B^2/2)) + q_s^{(\text{out})} c_F ((\zeta^2/2) - (D_B^2/2))$
$\phi_{s,1}(\zeta) = q_s^{(\text{in})} a_F \zeta^2 + q_s^{(\text{in})} b_F \zeta, \quad \phi_{s,2}(\zeta) = q_s^{(\text{out})} a_F \zeta^2 + q_s^{(\text{out})} b_F \zeta$ $\phi_{s,3}(\zeta) = q_s^{(\text{in})} c_F \zeta, \quad \phi_{s,4}(\zeta) = \phi_{s,5}(\zeta) = q_s^{(\text{out})} c_F \zeta$
$\mathcal{Q}_s(\xi) = q_s^{(\text{in})} a_K \mathcal{Q}_{s,1}(\xi) + q_s^{(\text{in})} b_K \mathcal{Q}_{s,2}(\xi) + q_s^{(\text{out})} a_K \mathcal{Q}_{s,3}(\xi) + q_s^{(\text{out})} b_K \mathcal{Q}_{s,4}(\xi) + q_s^{(\text{in})} c_K \mathcal{Q}_{s,5}(\xi)$ $+ q_s^{(\text{out})} c_K (\mathcal{Q}_{s,6}(\xi; \Theta_{\text{nlos}}) + \mathcal{Q}_{s,7}(\xi; \Theta_{\text{nlos}}))$
$\mathbb{1}_{B,K} = \mathbb{1}(D_B \leq D_K), \quad \mathbb{1}_{K,B} = \mathbb{1}(D_K \leq D_B), \quad \mathbb{1}_B(\xi) = \mathbb{1}((\xi/\kappa_s)^{1/\gamma_s} \leq D_B), \quad \mathbb{1}_K(\xi) = \mathbb{1}((\xi/\kappa_s)^{1/\gamma_s} \leq D_K)$
$\mathcal{Q}_{s,1}(\xi) = \mathcal{J}_2 \left(\xi; \theta = T\xi, \gamma = \gamma_s, n = 3, z = (1/\kappa_s)^{3/\gamma_s}, A = A_{s,1}, B = B_{s,1} \right)$ $\mathcal{Q}_{s,2}(\xi) = \mathcal{J}_2 \left(\xi; \theta = T\xi, \gamma = \gamma_s, n = 2, z = (1/\kappa_s)^{2/\gamma_s}, A = A_{s,2}, B = B_{s,2} \right)$
$\mathcal{Q}_{s,3}(\xi) = \mathcal{J}_2 \left(\xi; \theta = T\xi, \gamma = \gamma_s, n = 3, z = (1/\kappa_s)^{3/\gamma_s}, A = A_{s,3}(\xi), B = B_{s,3}(\xi) \right) \mathbb{1}_{B,K} \mathbb{1}_K(\xi)$ $\mathcal{Q}_{s,4}(\xi) = \mathcal{J}_2 \left(\xi; \theta = T\xi, \gamma = \gamma_s, n = 2, z = (1/\kappa_s)^{2/\gamma_s}, A = A_{s,4}(\xi), B = B_{s,4}(\xi) \right) \mathbb{1}_{B,K} \mathbb{1}_K(\xi)$
$\mathcal{Q}_{s,5}(\xi) = \mathcal{J}_2 \left(\xi; \theta = T\xi, \gamma = \gamma_s, n = 2, z = (1/\kappa_s)^{2/\gamma_s}, A = A_{s,5}(\xi), B = B_{s,5}(\xi) \right) \mathbb{1}_{K,B} \mathbb{1}_B(\xi)$ $\mathcal{Q}_{s,6}(\xi; \Theta_{\text{nlos}} \rightarrow \infty) = \mathcal{J}_1 \left(\xi; \theta = T\xi, \gamma = \gamma_s, n = 2, z = (1/\kappa_s)^{2/\gamma_s}, A = A_{s,6}(\xi) \right) \mathbb{1}_{B,K}$
$\mathcal{Q}_{s,7}(\xi; \Theta_{\text{nlos}} \rightarrow \infty) = \mathcal{J}_1 \left(\xi; \theta = T\xi, \gamma = \gamma_s, n = 2, z = (1/\kappa_s)^{2/\gamma_s}, A = A_{s,7}(\xi) \right) \mathbb{1}_{K,B}$ $\mathcal{Q}_{s,6}(\xi; \Theta_{\text{nlos}} = \kappa_{\text{nlos}} R_A^{\gamma_{\text{nlos}}}) = \mathcal{J}_2 \left(\xi; \theta = T\xi, \gamma = \gamma_s, n = 2, z = (1/\kappa_s)^{2/\gamma_s}, A = A_{s,6}(\xi), B = B_{s,6}(\xi) \right) \mathbb{1}_{B,K}$
$\mathcal{Q}_{s,7}(\xi; \Theta_{\text{nlos}} = \kappa_{\text{nlos}} R_A^{\gamma_{\text{nlos}}}) = \mathcal{J}_2 \left(\xi; \theta = T\xi, \gamma = \gamma_s, n = 2, z = (1/\kappa_s)^{2/\gamma_s}, A = A_{s,7}(\xi), B = B_{s,7}(\xi) \right) \mathbb{1}_{K,B}$ $A_{s,1}(\xi) = A_{s,2}(\xi) = \min\{\xi, \min\{\kappa_s D_K^{\gamma_s}, \kappa_s D_B^{\gamma_s}\}\}, \quad A_{s,3}(\xi) = A_{s,4}(\xi) = A_{s,7}(\xi) = \max\{\xi, \kappa_s D_B^{\gamma_s}\}$
$A_{s,5}(\xi) = A_{s,6}(\xi) = \max\{\xi, \kappa_s D_K^{\gamma_s}\}, \quad B_{s,1}(\xi) = B_{s,2}(\xi) = \min\{\kappa_s D_K^{\gamma_s}, \kappa_s D_B^{\gamma_s}\}$ $B_{s,3}(\xi) = B_{s,4}(\xi) = \kappa_s D_K^{\gamma_s}, \quad B_{s,5}(\xi) = \kappa_s D_B^{\gamma_s}, \quad B_{s,6}(\xi) = B_{s,7}(\xi) = \kappa_{\text{nlos}} R_A^{\gamma_{\text{nlos}}}$

single-ball blockage model in [9]. In particular, each BS-to-MT₀ link of length $r = \|x\|$, where x is the location of a generic BS, can be either in Line-Of-Sight (LOS) or in Non-Line-Of-Sight (NLOS) with a probability that depends only on the distance r . Blockage conditions between different links are assumed to be mutually independent. More precisely, the probability that a link of length r is in LOS is $p_{\text{los}}(r) = q_{\text{los}}^{(\text{in})} \mathbb{1}(r \leq D_B) + q_{\text{los}}^{(\text{out})} \mathbb{1}(r > D_B)$, where D_B is the radius of the so-called LOS-ball that depends on the area covered by blockages, and $0 \leq q_{\text{los}}^{(\text{in})} \leq 1$ and $0 \leq q_{\text{los}}^{(\text{out})} \leq 1$ are the probabilities that links of length smaller and larger than D_B , respectively, are in LOS. The probability that the same links are in NLOS is $p_{\text{nlos}}(r) = q_{\text{nlos}}^{(\text{in})} \mathbb{1}(r \leq D_B) + q_{\text{nlos}}^{(\text{out})} \mathbb{1}(r > D_B)$, with $p_{\text{los}}(r) + p_{\text{nlos}}(r) = q_{\text{los}}^{(\text{in})} + q_{\text{nlos}}^{(\text{in})} = q_{\text{los}}^{(\text{out})} + q_{\text{nlos}}^{(\text{out})} = 1$ for $r \geq 0$. The path-loss of LOS and NLOS links is $l_{\text{los}}(x) = \kappa_{\text{los}} \|x\|^{\gamma_{\text{los}}}$ and $l_{\text{nlos}}(x) = \kappa_{\text{nlos}} \|x\|^{\gamma_{\text{nlos}}}$, respectively, where $(\kappa_{\text{los}}, \gamma_{\text{los}})$ and $(\kappa_{\text{nlos}}, \gamma_{\text{nlos}})$ have the same meaning as in Section II-B.

The following theorem provides us with a tractable expression of the coverage probability in (6), by considering a

network model based on I-PPPs, a single-ball blockage model, and a cell association criterion based on the smallest path-loss. Since the BS-to-MT₀ links can be either in LOS or NLOS, the serving BS is not necessarily the nearest BS to the probe MT (see Section III-C and *Remark 12*). In particular, $\tilde{P}_{\text{cov}}^{(\text{o})}$ in (6) is formulated for two generic triplets of parameters (a_F, b_F, c_F) and (a_K, b_K, c_K) and, hence, it is applicable to network models with spatial inhibition and aggregation.

Theorem 2: In the presence of spatial blockages, $\tilde{P}_{\text{cov}}^{(\text{o})}$ in (6) can be formulated as follows:

$$\tilde{P}_{\text{cov}}^{(\text{o})} = \int_0^{\Theta_{\text{nlos}}} \exp(-\xi T \sigma_N^2 / P_{\text{tx}}) \times \exp(-2\pi\lambda_{BS} (\mathcal{Q}_{\text{los}}(\xi) + \mathcal{Q}_{\text{nlos}}(\xi))) \mathcal{U}_0(\xi) d\xi \quad (20)$$

where $\Theta_{\text{nlos}} \rightarrow \infty$ and $\Theta_{\text{nlos}} = \kappa_{\text{nlos}} R_A^{\gamma_{\text{nlos}}}$ for infinite-size and finite-size networks, respectively, and the rest of the functions are provided in Table IV for $s \in \{\text{los}, \text{nlos}\}$.

Proof: It follows similar to the proof of *Theorem 1*, since the superposition of two independent I-PPPs is an I-PPP whose intensity measure is the sum of the intensity measures

$$\text{SINR} = \frac{\left(P_{T1} g_{T1,0} / l_{T1} \left(x_{T1,0}^{(F)} \right) \right) \mathbb{1} \left(P_{T1} / l_{T1} \left(x_{T1,0} \right) \geq P_{T2} / l_{T2} \left(x_{T2,0} \right) \right)}{\sigma_N^2 + \sum_{x \in \Phi_{T1}^{(I)} \left(x_{T1,0}^{(F)} \right)} P_{T1} g_{T1,x} / l_{T1} \left(x \right) + \sum_{x \in \Phi_{T2}^{(I)} \left(x_{T2,0}^{(F)} \right)} P_{T2} g_{T2,x} / l_{T2} \left(x \right) + P_{T2} g_{T2,x} / l_{T2} \left(x_{T2,0}^{(F)} \right)} + \frac{\left(P_{T2} g_{T2,0} / l_{T2} \left(x_{T2,0}^{(F)} \right) \right) \mathbb{1} \left(P_{T2} / l_{T2} \left(x_{T2,0} \right) > P_{T1} / l_{T1} \left(x_{T1,0} \right) \right)}{\sigma_N^2 + \sum_{x \in \Phi_{T2}^{(I)} \left(x_{T2,0}^{(F)} \right)} P_{T2} g_{T2,x} / l_{T2} \left(x \right) + \sum_{x \in \Phi_{T1}^{(I)} \left(x_{T1,0}^{(F)} \right)} P_{T1} g_{T1,x} / l_{T1} \left(x \right) + P_{T1} g_{T1,x} / l_{T1} \left(x_{T1,0}^{(F)} \right)} \quad (21)$$

of the two I-PPPs. In particular, the intensity measures of the I-PPPs constituted by the links in LOS and NLOS are obtained from (9) by replacing $\lambda_{\text{BS}}^{(\cdot)}(\zeta)$ with $\lambda_{\text{BS}}^{(\cdot)}(\zeta) p_s(\zeta)$ for $s \in \{\text{los}, \text{nlos}\}$. \square

B. Multi-Tier Cellular Networks

In this section, we consider a two-tier cellular network. The tiers are denoted by T1 and T2. The BSs of tiers T1 and T2 belong to two independent and motion-invariant PPs that are denoted by Ψ_{T1} and Ψ_{T2} , respectively. The system model is the same as in Section II for single-tier cellular networks, with a few exceptions. Let $x \in \Psi_{\mathcal{T}}$ be the location of a BS of tier $\mathcal{T} \in \{\text{T1}, \text{T2}\}$. The path-loss at location x is $l_{\mathcal{T}}(x) = \kappa_{\mathcal{T}} \|x\|^{\gamma_{\mathcal{T}}}$, where $\kappa_{\mathcal{T}}$ and $\gamma_{\mathcal{T}}$ are the path-loss constant and slope of tier \mathcal{T} similar to Section II-B. The transmit power of tier \mathcal{T} is $P_{\mathcal{T}} = \delta_{\mathcal{T}} P_{\text{tx}}$, where $\delta_{\mathcal{T}} \geq 0$. A similar notation is employed for the other system parameters introduced in Section II. The cell association criterion is based on the highest average received power. More precisely, let $x_{\mathcal{T},0}$ be the location of the BS of tier \mathcal{T} that provides the smallest path-loss to the typical MT and that is computed by using (1). Then, the location of the serving BS of the typical MT of the two-tier cellular network is $x_{T1,0}$ if $P_{T1}/l_{T1}(x_{T1,0}) \geq P_{T2}/l_{T2}(x_{T2,0})$ and $x_{T2,0}$ otherwise. For ease of writing, we introduce the shorthand $\bar{\kappa}_{\mathcal{T}} = \kappa_{\mathcal{T}}/\delta_{\mathcal{T}}$ for $\mathcal{T} \in \{\text{T1}, \text{T2}\}$.

We apply the IDT approach for modeling the locations of the BSs of Ψ_{T1} and Ψ_{T2} . In particular, each motion-invariant PP is approximated by using two I-PPPs, which, similar to Section III, are denoted by $(\Phi_{T1}^{(F)}, \Phi_{T1}^{(K)})$ and $(\Phi_{T2}^{(F)}, \Phi_{T2}^{(K)})$. The parameters of each pair of I-PPPs are obtained as described in Section III. In simple terms, each motion-invariant PP is approximated, from the standpoint of the typical MT, with two I-PPPs as if it was the only tier of the cellular network. The BS of tier $\mathcal{T} \in \{\text{T1}, \text{T2}\}$ that provides that smallest path-loss among all the BSs of tier \mathcal{T} and the corresponding I-PPP of conditionally independent interfering BSs are defined similar to (5), and are denoted by $x_{\mathcal{T},0}^{(F)} \in \Phi_{\mathcal{T}}^{(F)}$ and $\Phi_{\mathcal{T}}^{(I)} = \Phi_{\mathcal{T}}^{(I)}(x_{\mathcal{T},0}^{(F)}) \subseteq \Phi_{\mathcal{T}}^{(K)}$. Similar to (6), the coverage probability of a two-tier cellular network is $\tilde{P}_{\text{cov}}^{(o)} = \Pr\{\text{SINR} > T\}$, where the SINR is in (21) shown at the top of this page.

Remark 20: The direct inspection of the SINR in (21) highlights the fundamental difference between the proposed IDT approach based on conditionally independent I-PPPs and

the conventional modeling approach based on H-PPPs. Let us consider the first line of the SINR in (21), i.e., the probe MT is served by a BS that belongs to tier T1. Similar comments apply to the second line of (21). The interference in the denominator is the sum of three terms: i) the second addend in the denominator is the interference that originates from the BSs of tier T1, whose path-loss is greater than the path-loss of the serving BS at location $x_{T1,0}^{(F)}$, ii) the third addend in the denominator is the interference that originates from the BSs of tier T2, whose path-loss is greater than the path-loss of the BS of tier T2 that is at location $x_{T2,0}^{(F)}$, instead of at location $x_{T1,0}^{(F)}$ as is the case in models based on H-PPPs, and iii) the fourth addend in the denominator is the interference that originates from the BS of tier T2 at location $x_{T2,0}^{(F)}$, which is not treated separately in models based on H-PPPs. These differences with respect to spatial models based on H-PPPs are specific of the IDT approach and are necessary because the serving BS and the interfering BSs of each tier are obtained from conditionally independent I-PPPs with different spatial inhomogeneities. In models based on H-PPPs, on the other hand, all the BSs are generated from a single H-PPP. In the IDT approach, these differences in the third and fourth term of the denominator of the SINR ensure that the path-loss of the interfering BSs that belong to $\Phi_{T2}^{(I)}(x_{T2,0}^{(F)})$ is not smaller than the path-loss of the BS at location $x_{T2,0}^{(F)}$, even if it is not the serving BS of the two-tier cellular network. This condition is essential for appropriately reproducing the spatial interactions among the BSs of the original motion-invariant PP. Stated differently, the SINR in (21) is conditioned upon the locations $x_{T1,0}^{(F)}$ and $x_{T2,0}^{(F)}$, while in spatial models based on H-PPPs the conditioning is needed only upon the location of the serving BS, i.e., either upon $x_{T1,0}^{(F)}$ or $x_{T2,0}^{(F)}$ only. \square

The following theorem yields the coverage probability of the two-tier cellular network based on (21).

Theorem 3: In two-tier cellular networks, $\tilde{P}_{\text{cov}}^{(o)}$ in (21) can be formulated as in (22) shown at the bottom of the next page, where, for $\mathcal{T} \in \{\text{T1}, \text{T2}\}$, $\Theta_{\mathcal{T}} \rightarrow \infty$ and $\Theta_{\mathcal{T}} = \bar{\kappa}_{\mathcal{T}} R_A^{\gamma_{\mathcal{T}}}$ for infinite-size and finite-size networks, respectively, $\mathcal{W}_1(\xi_1, \xi_2) = \mathcal{S}_{T1}(\xi_1, \xi_1) + \mathcal{S}_{T2}(\xi_2, \xi_1)$, $\mathcal{W}_2(\xi_1, \xi_2) = \mathcal{S}_{T1}(\xi_1, \xi_2) + \mathcal{S}_{T2}(\xi_2, \xi_2)$, and the rest of the functions are given in Table V for $\mathcal{T} \in \{\text{T1}, \text{T2}\}$.

Proof: It follows similar to the proof of *Theorem 1*, by taking into account that the addends in the denominator of the SINR are independent by conditioning on $x_{T1,0}^{(F)}$ and $x_{T2,0}^{(F)}$. \square

TABLE V
AUXILIARY FUNCTIONS USED IN *Theorem 3* ($\mathcal{U}_{\text{IN}}(\cdot)$, $\mathcal{U}_{\text{OUT}}(\cdot)$, AND $\mathcal{I}_{(\cdot)}(\cdot)$ ARE DEFINED IN TABLE III)

Function Definition ($\Pi_{\mathcal{T}} = \{\kappa = \bar{\kappa}_{\mathcal{T}}, \gamma = \gamma_{\mathcal{T}}, a_{\text{F}} = a_{\mathcal{T},\text{F}}, b_{\text{F}} = b_{\mathcal{T},\text{F}}, c_{\text{F}} = c_{\mathcal{T},\text{F}}\}$)
$\mathcal{U}_{\mathcal{T},0}(\xi) = \mathcal{U}_{\text{IN}}(\xi; \Pi_{\mathcal{T}}) \mathbb{1}(\xi \leq \bar{\kappa}_{\mathcal{T}}((c_{\mathcal{T},\text{F}} - b_{\mathcal{T},\text{F}})/a_{\mathcal{T},\text{F}})^{\gamma_{\mathcal{T}}}) + \mathcal{U}_{\text{OUT}}(\xi; \Pi_{\mathcal{T}}) \mathbb{1}(\xi \geq \bar{\kappa}_{\mathcal{T}}((c_{\mathcal{T},\text{F}} - b_{\mathcal{T},\text{F}})/a_{\mathcal{T},\text{F}})^{\gamma_{\mathcal{T}}})$ $\mathcal{S}_{\mathcal{T}}(x, y; \Theta \rightarrow \infty) = \mathcal{I}_1(x; \Pi_{\mathcal{T}}, T = T = Ty/x) + \mathcal{I}_2(x; \Pi_{\mathcal{T}}, T = T = Ty/x) + \mathcal{I}_3(x; \Pi_{\mathcal{T}}, T = Ty/x)$ $\quad + \mathcal{I}_4(x; \Pi_{\mathcal{T}}, T = Ty/x) + \mathcal{I}_5(x; \Pi_{\mathcal{T}}, T = T = Ty/x) + \mathcal{I}_6(x; \Pi_{\mathcal{T}}, T = Ty/x)$ $\mathcal{S}_{\mathcal{T}}(x, y; \Theta_{\mathcal{T}} = \bar{\kappa}_{\mathcal{T}} R_{\text{A}}^{\gamma_{\mathcal{T}}}) = \mathcal{I}_1(x; \Pi_{\mathcal{T}}, T = T = Ty/x) + \mathcal{I}_2(x; \Pi_{\mathcal{T}}, T = T = Ty/x) + \mathcal{I}_3(x; \Pi_{\mathcal{T}}, T = Ty/x)$ $\quad + \mathcal{I}_4(x; \Pi_{\mathcal{T}}, T = Ty/x) + \mathcal{I}_7(x; \Pi_{\mathcal{T}}, T = T = Ty/x) + \mathcal{I}_8(x; \Pi_{\mathcal{T}}, T = T = Ty/x)$ $\quad + \mathcal{I}_9(x; \Pi_{\mathcal{T}}, T = T = Ty/x) + \mathcal{I}_{10}(x; \Pi_{\mathcal{T}}, T = Ty/x)$

TABLE VI
EMPIRICAL PPs (ISD = INTER-SITE DISTANCE). THEIR PARAMETERS ARE DEFINED IN THE REFERENCES

Point Process	Parameters
DPP (Cauchy, Los Angeles) [23]	$\lambda_{\text{BS}} = 0.2346 \text{ BS/km}^2, \alpha = 2.13, \mu = 3.344, \text{Area} = 28 \times 28 \text{ km}^2$
DPP (Cauchy, Houston) [23]	$\lambda_{\text{BS}} = 0.4490 \text{ BS/km}^2, \alpha = 1.558, \mu = 3.424, \text{Area} = 16 \times 16 \text{ km}^2$
DPP (Gaussian, Los Angeles) [23]	$\lambda_{\text{BS}} = 0.2345 \text{ BS/km}^2, \alpha = 1.165, \text{Area} = 28 \times 28 \text{ km}^2$
DPP (Gaussian, Houston) [23]	$\lambda_{\text{BS}} = 0.4492 \text{ BS/km}^2, \alpha = 0.8417, \text{Area} = 16 \times 16 \text{ km}^2$
GPP (Urban, $\beta = 0.900$) [20]	$\lambda_{\text{BS}} = 31.56 \text{ BS/km}^2, \text{Area} = 3.784^2 \pi \text{ km}^2, \gamma = 3.5$
GPP (Urban, $\beta = 0.925$) [20]	$\lambda_{\text{BS}} = 31.56 \text{ BS/km}^2, \text{Area} = 3.784^2 \pi \text{ km}^2, \gamma = \{2.5, 4\}$
GPP (Urban, $\beta = 0.975$) [20]	$\lambda_{\text{BS}} = 31.56 \text{ BS/km}^2, \text{Area} = 3.784^2 \pi \text{ km}^2, \gamma = 3$
GPP (Rural, $\beta = 0.200$) [20]	$\lambda_{\text{BS}} = 0.03056 \text{ BS/km}^2, \text{Area} = 124.578^2 \pi \text{ km}^2, \gamma = 3.5$
GPP (Rural, $\beta = 0.225$) [20]	$\lambda_{\text{BS}} = 0.03056 \text{ BS/km}^2, \text{Area} = 124.578^2 \pi \text{ km}^2, \gamma = \{3, 4\}$
GPP (Rural, $\beta = 0.375$) [20]	$\lambda_{\text{BS}} = 0.03056 \text{ BS/km}^2, \text{Area} = 124.578^2 \pi \text{ km}^2, \gamma = 2.5$
Lattice PP	$\text{ISD} = \{100, 200, 300, 500\} \text{ m}$
Perturbed Lattice PP (ISD = 100 m)	$s = \{50, 80, 100, 200\} \text{ m}$
LGCP (Urban) [27] (exp. cov.)	$\lambda_{\text{BS}} = 4 \text{ BS/km}^2, \beta = 0.03, \sigma^2 = 3.904, \mu = -0.5634, \text{Area} = 20 \times 20 \text{ km}^2$
LGCP (London) [27] (exp. cov.)	$\lambda_{\text{BS}} = 9.919 \text{ BS/km}^2, \beta = 0.054, \sigma^2 = 2.0561, \mu = 1.2665, \text{Area} = 6 \times 6 \text{ km}^2$
LGCP (Warsaw) [27] (exp. cov.)	$\lambda_{\text{BS}} = 27.36 \text{ BS/km}^2, \beta = 0.0288, \sigma^2 = 2.7228, \mu = 1.9477, \text{Area} = 8 \times 8 \text{ km}^2$
PHP [26]	$R_{\text{cell}} = 0.5 \text{ km}, \lambda_{\text{hole}} = 0.005 \lambda_{\text{BS}} \text{ BS/km}^2, R_{\text{hole}} = 4 \text{ km}$
PHP [26]	$R_{\text{cell}} = 0.1 \text{ km}, \lambda_{\text{hole}} = 0.005 \lambda_{\text{BS}} \text{ BS/km}^2, R_{\text{hole}} = 0.8 \text{ km}$
MCP [45]	$R_{\text{cell}} = R_{\text{parent}} = 0.25 \text{ km}, R_{\text{offspring}} = 50 \text{ m}, \text{Average number offsprings} = 5$

Remark 21: Compared with *Theorem 1* and *Theorem 2*, the coverage probability in (22) is formulated in terms of a two-fold integral. This originates from *Remark 20* and, more precisely, from the fact that the SINR in (21) depends on the locations of the BSs of each tier that provide, in their own tier, the smallest path-loss to the probe MT. Simple bounds may be used to obtain a single-integral expression of the coverage probability. This study is, however, outside the scope of this paper due to space limitations. In addition, the computation of (22) is sufficiently simple for two-tier networks. Simple bounds may, on the other hand, be needed if more than two tiers are considered. In general, the number of fold integrals coincides with the number of tiers. \square

Remark 22: In *Theorem 2* and *Theorem 3*, the spatial inhomogeneities of the I-PPPs are the same as in *Theorem 1*. They depend only on the spatial characteristics of the original

motion-invariant PP and are independent of, e.g., blockages and LOS/NLOS channel parameters. \square

VI. NUMERICAL AND SIMULATION RESULTS

In this section, we illustrate several numerical results that substantiate the applicability of the IDT approach for the modeling and analysis of practical cellular network deployments. The network deployments considered in our study are reported in Table VI. The simulation setup is summarized in Table VII. Table VIII reports the algorithm used for simulating the IDT approach in the general case of a two-tier cellular network. Table IX and Table X provide the triplets of parameters ($a_{\text{F}}, b_{\text{F}}, c_{\text{F}}$) and ($a_{\text{K}}, b_{\text{K}}, c_{\text{K}}$) of the IDT approach that correspond to the PPs in Table VI and that exhibit spatial inhibition and spatial aggregation, respectively. These triplets

$$\begin{aligned}
\tilde{P}_{\text{cov}}^{(\circ)} = & \int_0^{\Theta_{\text{T1}}} \left(\int_{\xi_1}^{\Theta_{\text{T2}}} e^{-\xi_1 T \sigma_{\text{N}}^2 / P_{\text{tx}}} (1 + T(\xi_1 / \xi_2))^{-1} e^{-\mathcal{W}_1(\xi_1, \xi_2)} \mathcal{U}_{\text{T2},0}(\xi_2) d\xi_2 \right) \mathcal{U}_{\text{T1},0}(\xi_1) d\xi_1 \\
& + \int_0^{\Theta_{\text{T2}}} \left(\int_{\xi_2}^{\Theta_{\text{T1}}} e^{-\xi_1 T \sigma_{\text{N}}^2 / P_{\text{tx}}} (1 + T(\xi_2 / \xi_1))^{-1} e^{-\mathcal{W}_2(\xi_1, \xi_2)} \mathcal{U}_{\text{T1},0}(\xi_1) d\xi_1 \right) \mathcal{U}_{\text{T2},0}(\xi_2) d\xi_2 \quad (22)
\end{aligned}$$

TABLE VII
SETUP OF PARAMETERS (UNLESS OTHERWISE STATED)

Parameter	Value ($k = \times 1000$)
γ	{2.5, 3.5}
$\kappa = (4\pi f_c/3 \cdot 10^8)^2$	$f_c = 2.1$ GHz
σ_N^2	0 Watt
P_{tx}	1 Watt
λ_{BS}	$1/(\pi R_{cell}^2)$ BSs/km ²
Two-tier network	$\delta_{T1} = \delta_{T2} = 1$ $\tau_{T1} = \tau_{T2} = 1$ $\gamma_{T1} = \gamma_{T2} = \gamma$
$\gamma_{los}, \gamma_{nlos}$	2.5, 3.5
D_B [10]	109.8517 m
$q_{los}^{(in)}, q_{nlos}^{(in)}$ [10]	0.7196, 0.0002
Functions for sim. in R	dppCauchy, dppGauss rLGCP
Simulations of GPPs	[46, Proposition 4.3]
Simulations of other PPs	Based on definition [30]
Perturbed Lattice	Rand shift in $(-s/2, s/2)$
Number of realizations	DPP: 100k, GPP: 10k
Number of realizations	LGCP: 20k, 30k (London)
Number of realizations	PHP: 20k, MCPP: 10k
Number of realizations	Lattice: 10k
Number of realizations	Perturbed Lattice: 15k

TABLE VIII
SIMULATION OF THE IDT APPROACH (TWO-TIER, PPs
WITH REPULSION OR CLUSTERING)

1. Generate a H-PPP with intensity $\lambda_{T1} \max\{1, c_{T1,F}\}$
2. Thin the obtained H-PPP with ret. prob. in (10), (11)
3. Generate a H-PPP with intensity $\lambda_{T2} \max\{1, c_{T2,F}\}$
4. Thin the obtained H-PPP with ret. prob. in (10), (11)
5. Apply the path-loss and fading models
6. Compute the average received (rx) power from all BSs
7. Identify the BSs of each tier ($BS_{T1,0}, BS_{T2,0}$)
providing the best average rx power in their own tier
8. Identify the serving BS (BS_0) (best average rx power)
9. Remove all BSs except $BS_{T1,0}$ and $BS_{T2,0}$
10. Generate a H-PPP with intensity $\lambda_{T1} \max\{1, c_{T1,K}\}$
11. Thin the obtained H-PPP with ret. prob. in (10), (11)
12. Generate a H-PPP with intensity $\lambda_{T2} \max\{1, c_{T2,K}\}$
13. Thin the obtained H-PPP with ret. prob. in (10), (11)
14. Apply the path-loss and fading models
15. Compute the average rx power from all BSs
16. Remove all BSs of T1 (T2) whose average rx power is higher than that of $BS_{T1,0}$ ($BS_{T2,0}$)
17. Compute the coverage probability

of parameters are obtained by solving (14). As mentioned in *Remark 14*, the optimization problem in (14) is solved with the aid of the `lsqcurvefit` function that is available in Matlab. Since the solution of (14) depends on the initialization point of the algorithm, no general conclusions about the global optimality of the solution can be drawn. There may exist

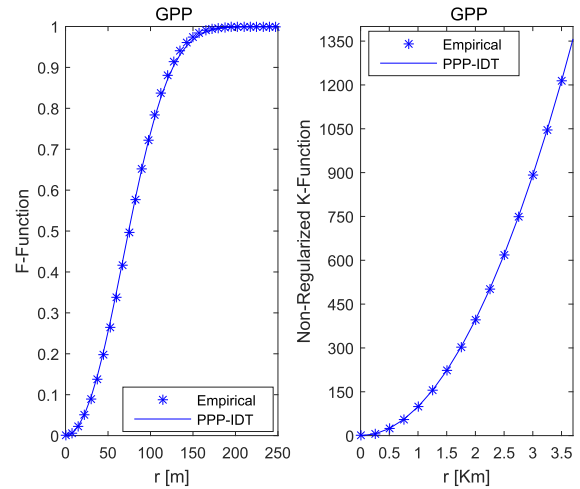


Fig. 1. F-function and non-regularized K-function of GPP-Urban ($\beta = 0.9$). Markers: Monte Carlo simulations. Solid lines: IDT approach from (14).

multiple triplets of parameters that provide sufficiently good estimates for the F-function and non-regularized K-function. The triplets of parameters reported in Table IX and Table X are obtained by solving (14) for several random starting points of the search and by choosing the solution that provides the smallest error value. It is worth noting that the triplets of parameters reported in Tables IX and X are expressed in terms of a large number of decimal figures, as provided by Matlab to us. An important issue is to study the number of *significant* figures that are necessary to retain a good accuracy. Even though this comprehensive study is outside the scope of the present paper, our empirical trials have shown that three⁴ significant figures may be sufficient to estimate the coverage probability in the considered case studies. By direct inspection of Table IX and Table X, we evince, notably, that all the triplets of parameters satisfy the constraints stated in *Lemma 5* and *Lemma 6*.

In Fig. 1, we compare the F-function and non-regularized K-function of the original PP against those obtained by using the IDT approach. The curve labelled “Empirical” is obtained by generating the data set in Table VI (GPP-Urban with $\beta = 0.9$) with the aid of the simulation method in [46]. The curve labelled “PPP-IDT” is obtained by using the triplets of parameters, (a_F, b_F, c_F) and (a_K, b_K, c_K) , reported in Table IX. We note an almost perfect overlap between the curves. The results, in addition, are in agreement with the analytical expressions in [20]. In Fig. 2, we consider a GPP and depict the triplet of parameters (a_F, b_F, c_F) as a function of β . The figure is obtained by solving (14) for different values of β and plotting the outcome. The best polynomial fitting of sixth degree is shown as well, along with the set of polynomial coefficients. Figure 2 brings to our attention that the optimization problem in (14) may be solved just once as a function of some sample values for the parameters that determine the spatial characteristics of the PP of interest. With these empirical samples at hand, the analytical relation

⁴Leading zeros are considered to be never significant.

TABLE IX
PARAMETERS OF THE IDT APPROACH (SPATIAL INHIBITION). $\check{a}_{(\cdot)}$ IS MEASURED IN 1/METER

Point Process	F-Function ($\check{a}_F, \check{b}_F, \check{c}_F$)	Non-regularized K-Function ($\check{a}_K, \check{b}_K, \check{c}_K$)
DPP (Cauchy, $\alpha = 2.13, \mu = 3.344$)	$\check{a}_F = 0.242792313440063 \cdot 10^{-3}$ $\check{b}_F = 1.00000000050633$ $\check{c}_F = 1.29043878627270$	$\check{a}_K = 0.665312376961223 \cdot 10^{-3}$ $\check{b}_K = 0.0800803505151663$ $\check{c}_K = 0.999966929758115$
DPP (Cauchy, $\alpha = 1.558, \mu = 3.424$)	$\check{a}_F = 0.329932369708525 \cdot 10^{-3}$ $\check{b}_F = 1.0000000203162$ $\check{c}_F = 1.31414585197489$	$\check{a}_K = 0.925771720753051 \cdot 10^{-3}$ $\check{b}_K = 0.0762137545180777$ $\check{c}_K = 0.999929848546426$
DPP (Gaussian, $\alpha = 1.165$)	$\check{a}_F = 0.257595475141932 \cdot 10^{-3}$ $\check{b}_F = 1.00000000000057$ $\check{c}_F = 1.46642395259731$	$\check{a}_K = 0.694526986147307 \cdot 10^{-3}$ $\check{b}_K = 0.00800453473629913$ $\check{c}_K = 0.999975490615518$
DPP (Gaussian, $\alpha = 0.8417$)	$\check{a}_F = 0.374139244964067 \cdot 10^{-3}$ $\check{b}_F = 1.0000000128277$ $\check{c}_F = 1.36923913017716$	$\check{a}_K = 0.963443744411944 \cdot 10^{-3}$ $\check{b}_K = 0.00642945511811224$ $\check{c}_K = 0.999947574776537$
GPP (Urban, $\beta = 0.900$)	$\check{a}_F = 0.00541280337683543$ $\check{b}_F = 1.0000000117948$ $\check{c}_F = 2.50742980678854$	$\check{a}_K = 0.00756610000002220$ $\check{b}_K = 0.0140800000000222$ $\check{c}_K = 0.999592878386863$
GPP (Urban, $\beta = 0.925$)	$\check{a}_F = 0.00556558536499347$ $\check{b}_F = 1.0000000213305$ $\check{c}_F = 2.52897621056288$	$\check{a}_K = 0.00839000000002220$ $\check{b}_K = 0.0200000000000222$ $\check{c}_K = 0.999432788402679$
GPP (Urban, $\beta = 0.975$)	$\check{a}_F = 0.00586932401892805$ $\check{b}_F = 1.00000000000032$ $\check{c}_F = 2.68047204883343$	$\check{a}_K = 0.0110000000000222$ $\check{b}_K = 0.0220000000000222$ $\check{c}_K = 0.999243424300274$
GPP (Rural, $\beta = 0.200$)	$\check{a}_F = 3.99946182077498 \cdot 10^{-5}$ $\check{b}_F = 1.01187371832462$ $\check{c}_F = 1.09948962377999$	$\check{a}_K = 0.000393029018145069$ $\check{b}_K = 0.0119099442149286$ $\check{c}_K = 0.99999841554118$
GPP (Rural, $\beta = 0.225$)	$\check{a}_F = 4.55473414133037 \cdot 10^{-5}$ $\check{b}_F = 1.01046879386340$ $\check{c}_F = 1.11306423054186$	$\check{a}_K = 0.000400570907629641$ $\check{b}_K = 0.0118898483733152$ $\check{c}_K = 0.99999810503409$
GPP (Rural, $\beta = 0.375$)	$\check{a}_F = 7.70128856239657 \cdot 10^{-5}$ $\check{b}_F = 1.00008049409712$ $\check{c}_F = 1.20464553702679$	$\check{a}_K = 0.000307206032822900$ $\check{b}_K = 0.0115923088272291$ $\check{c}_K = 0.99999586686943$
Square Lattice PP (ISD = 100 m)	$\check{a}_F = 0.0207235184299602$ $\check{b}_F = 1.00000000082389$ $\check{c}_F = 3.41775011845349$	$\check{a}_K = 0.0118573992067738$ $\check{b}_K = 0.0149219005445405$ $\check{c}_K = 0.997367566628052$
Square Lattice PP (ISD = 200 m)	$\check{a}_F = 0.0099918083369655$ $\check{b}_F = 1.00000000002186$ $\check{c}_F = 3.63796045765400$	$\check{a}_K = 0.00602053889182973$ $\check{b}_K = 0.0109873341685464$ $\check{c}_K = 0.997289630566070$
Square Lattice PP (ISD = 300 m)	$\check{a}_F = 0.00730786485041804$ $\check{b}_F = 1.0000000012366$ $\check{c}_F = 3.44527120081689$	$\check{a}_K = 0.00400186899997780$ $\check{b}_K = 0.010543399999778$ $\check{c}_K = 0.997319599926028$
Square Lattice PP (ISD = 500 m)	$\check{a}_F = 0.00474472289002515$ $\check{b}_F = 1.0000000000824$ $\check{c}_F = 3.53814219593121$	$\check{a}_K = 0.0025219999997779$ $\check{b}_K = 0.0060488999997780$ $\check{c}_K = 0.997261998863274$
Perturbed Square Lattice PP (ISD = 100 m, $s = 50$ m)	$\check{a}_F = 0.0181658635128918$ $\check{b}_F = 1.00000000000021$ $\check{c}_F = 4.60752972334688$	$\check{a}_K = 0.0129466213900222$ $\check{b}_K = 0.000494280313522204$ $\check{c}_K = 0.999994017100022$
Perturbed Square Lattice PP (ISD = 100 m, $s = 80$ m)	$\check{a}_F = 0.0130930488111834$ $\check{b}_F = 1.00000000000031$ $\check{c}_F = 3.20010528739824$	$\check{a}_K = 0.0140654251604636$ $\check{b}_K = 2.46971640043504 \cdot 10^{-5}$ $\check{c}_K = 0.999900000000028$
Perturbed Square Lattice PP (ISD = 100 m, $s = 100$ m)	$\check{a}_F = 0.0103067900650113$ $\check{b}_F = 1.00000000000014$ $\check{c}_F = 2.91053470488163$	$\check{a}_K = 0.0155243532394600$ $\check{b}_K = 0.0896282408085201$ $\check{c}_K = 0.999998682982071$
Perturbed Square Lattice PP (ISD = 100 m, $s = 200$ m)	$\check{a}_F = 0.00306137002539188$ $\check{b}_F = 1.00000000010676$ $\check{c}_F = 1.49061628381950$	$\check{a}_K = 0.000502260825187898$ $\check{b}_K = 0.950000006514566$ $\check{c}_K = 0.999918748989183$

between the triplet of parameters (a, b, c) may be obtained through polynomial fitting and then used for further analysis. This confirms, once again, the usefulness of the proposed IDT approach.

The numerical results of P_{cov} are reported in Figs. 3-11, by considering single-tier, single-tier with spatial blockages, and two-tier cellular network models. In each figure, Monte Carlo simulations are compared against the analytical frameworks in *Theorems 1-3*. As far as the system setups with

a small path-loss exponent ($\gamma = 2.5$ or $\gamma_{\text{los}} = 2.5$) are concerned, the analytical frameworks for finite-size networks are employed and R_A is set according to the data set being considered. In all the other cases, the analytical frameworks for infinite-size networks are used. Three curves are shown in each figure: i) the curve labelled ‘‘Empirical (R)’’ is obtained by generating the data sets listed in Table VI by using R [30], as described in Table VII. The data sets are imported in Matlab and the coverage is obtained through Monte Carlo simulations.

TABLE X
PARAMETERS OF THE IDT APPROACH (SPATIAL AGGREGATION). $\hat{a}_{(\cdot)}$ IS MEASURED IN 1/METER

Point Process	F-Function ($\hat{a}_F, \hat{b}_F, \hat{c}_F$)	Non-regularized K-Function ($\hat{a}_K, \hat{b}_K, \hat{c}_K$)
LGCP (Urban)	$\hat{a}_F = 3.00375582041718 \cdot 10^{-3}$ $\hat{b}_F = 0.999992970565002$ $\hat{c}_F = 0.660720583433523$	$\hat{a}_K = 0.25459999969997 \cdot 10^{-3}$ $\hat{b}_K = 1.17267857000002$ $\hat{c}_K = 1.00000000000042$
LGCP (London)	$\hat{a}_F = 0.87203489061171 \cdot 10^{-3}$ $\hat{b}_F = 0.952946863802724$ $\hat{c}_F = 0.833199670592430$	$\hat{a}_K = 13.7046788332358 \cdot 10^{-3}$ $\hat{b}_K = 2.77639999999998$ $\hat{c}_K = 1.00029311985637$
LGCP (Warsaw)	$\hat{a}_F = 5.10628352398303 \cdot 10^{-3}$ $\hat{b}_F = 0.999824829657571$ $\hat{c}_F = 0.729485294280125$	$\hat{a}_K = 14.7874237000000 \cdot 10^{-3}$ $\hat{b}_K = 2.39829157458606$ $\hat{c}_K = 1.00029112312127$
PHP ($R_{\text{cell}} = 0.5$ km)	$\hat{a}_F = 0.000770314253268006$ $\hat{b}_F = 0.99999999999976$ $\hat{c}_F = 0.0678028660887278$	$\hat{a}_K = 0.108972391052896$ $\hat{b}_K = 1.08148939349424$ $\hat{c}_K = 1.00074049690423$
PHP ($R_{\text{cell}} = 0.1$ km)	$\hat{a}_F = 0.00367373961597854$ $\hat{b}_F = 0.999999999999536$ $\hat{c}_F = 0.0674022684094626$	$\hat{a}_K = 9.86901285512281 \cdot 10^{-5}$ $\hat{b}_K = 1.02157321229225$ $\hat{c}_K = 1.00000000000002$
MCCP	$\hat{a}_F = 0.00260812705267213$ $\hat{b}_F = 0.433658802204551$ $\hat{c}_F = 0.221800647669995$	$\hat{a}_K = 0.204207885269187$ $\hat{b}_K = 24.6848802362645$ $\hat{c}_K = 1.009542056416424$

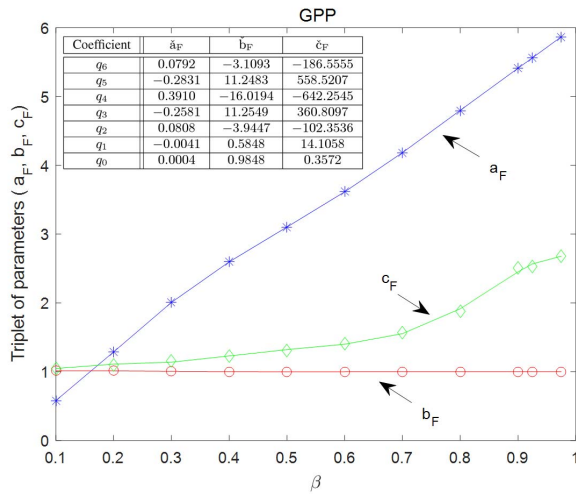


Fig. 2. Triplet of parameters ($\hat{a}_F, \hat{b}_F, \hat{c}_F$) for a GPP as a function of β . The parameter \hat{a}_F is multiplied by 1000. The table provides the best polynomial fitting of sixth order, e.g., $\hat{a}_F = \sum_{n=0}^6 q_n \beta^n$. Markers: Solution of (14). Solid lines: Best polynomial fitting.

The data sets of the GPP are obtained by using the simulation method in [46]; ii) the curve labelled “PPP-IDT” is obtained by using the IDT approach with the triplets of parameters listed in Table IX and Table X. Monte Carlo simulations are obtained in Matlab by using the algorithm reported in Table VIII. The analytical frameworks are computed with Mathematica; and iii) the curve labelled “PPP-H” corresponds to the benchmark cellular network deployments where the BSs are distributed according to H-PPPs. The analytical frameworks are obtained from *Theorems 1-3* according to *Remark 8*. As far as two-tier cellular networks are concerned, in particular, two independent H-PPPs of the same densities as the original motion-invariant PPs are considered. Figure 3 shows the coverage probability for its entire range of values, i.e., $[0, 1]$, and confirms the good accuracy offered by the IDT approach. To better highlight the gap between the curves labelled PPP-IDT and PPP-H, the other figures depict only the main body of the coverage probability.

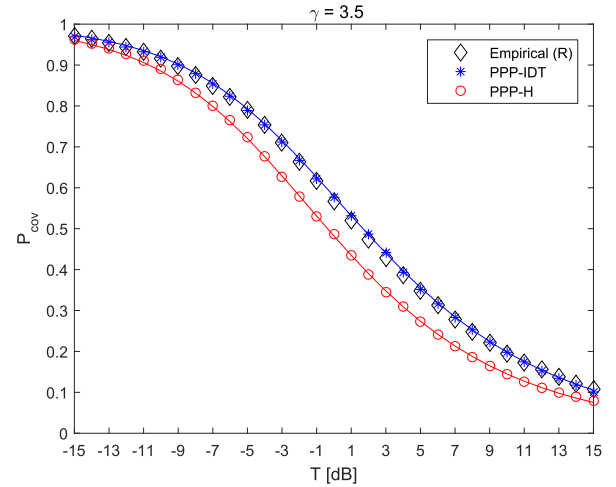


Fig. 3. P_{cov} of GPP-Urban ($\beta = 0.9$). Markers: Monte Carlo simulations. Solid lines: Analytical frameworks in *Theorem 1*.

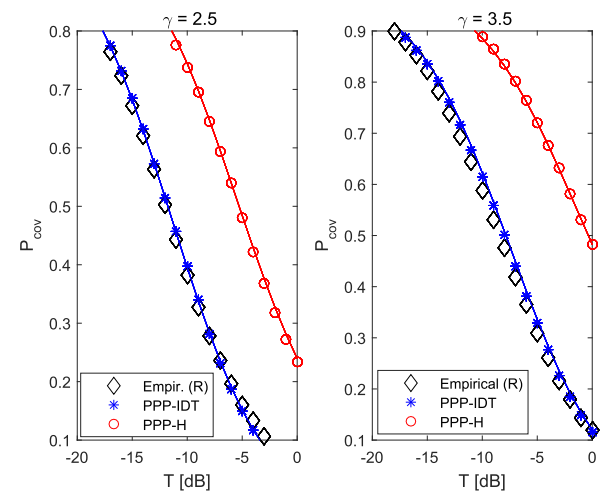


Fig. 4. P_{cov} of MCCP. Markers: Monte Carlo simulations. Solid lines: Analytical frameworks in *Theorem 1*.

From Figs. 4-11, we evince that the IDT approach is accurate, tractable, and capable of reproducing the spatial interactions of several PPs widely used for modeling the

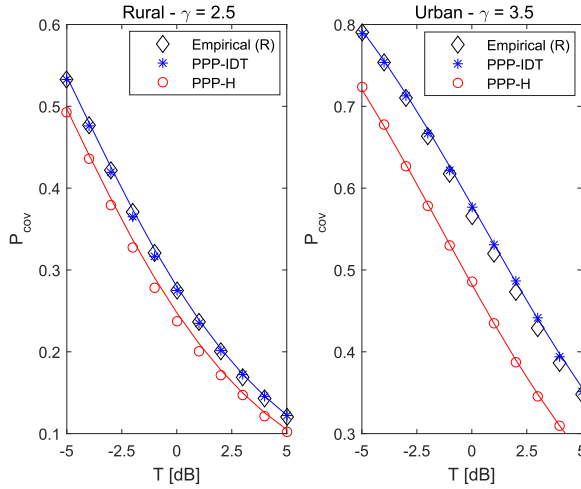


Fig. 5. P_{cov} of GPP-Rural ($\beta = 0.375$) and GPP-Urban ($\beta = 0.9$). Markers: Monte Carlo simulations. Solid lines: Analytical frameworks in *Theorem 1*.

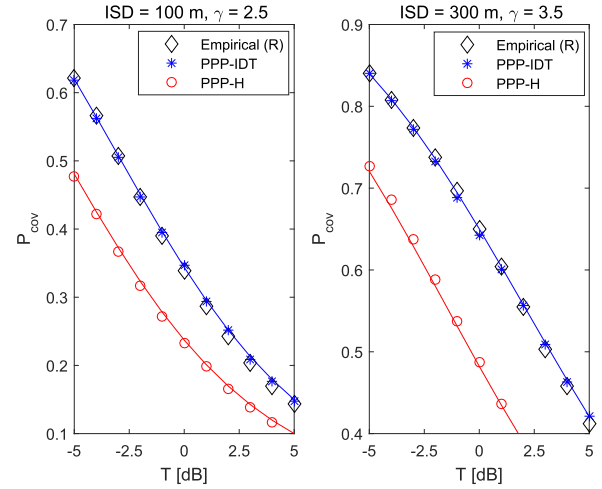


Fig. 8. P_{cov} of Square-Lattice (ISD = 100m, 300m). Markers: Monte Carlo simulations. Solid lines: Analytical frameworks in *Theorem 1*.

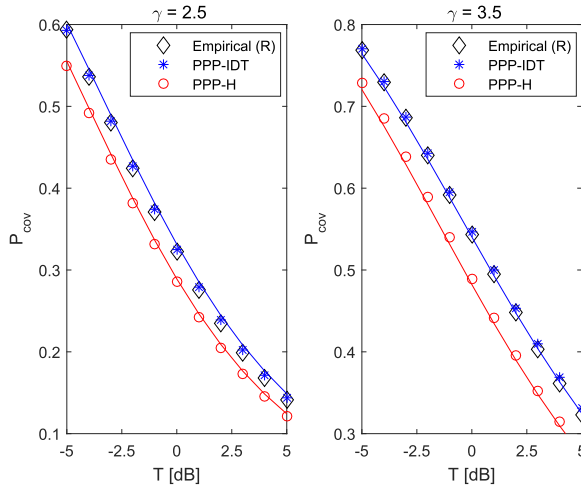


Fig. 6. P_{cov} of DPP-Cauchy (Houston). Markers: Monte Carlo simulations. Solid lines: Analytical frameworks in *Theorem 1*.

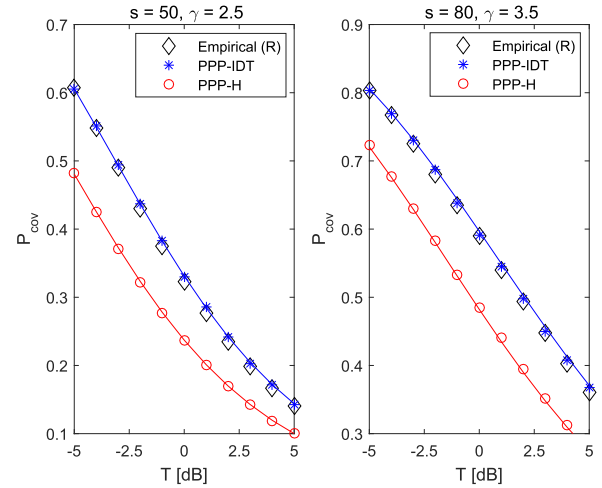


Fig. 9. P_{cov} of Perturbed-Square-Lattice (ISD = 100m). Markers: Monte Carlo simulations. Solid lines: Analytical frameworks in *Theorem 1*.

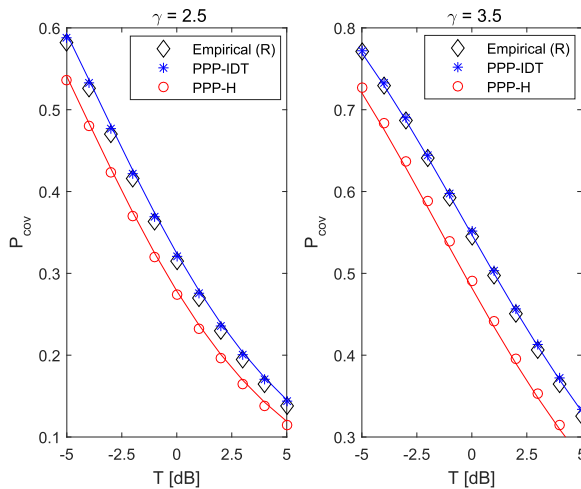


Fig. 7. P_{cov} of DPP-Gaussian (LA). Markers: Monte Carlo simulations. Solid lines: Analytical frameworks in *Theorem 1*.

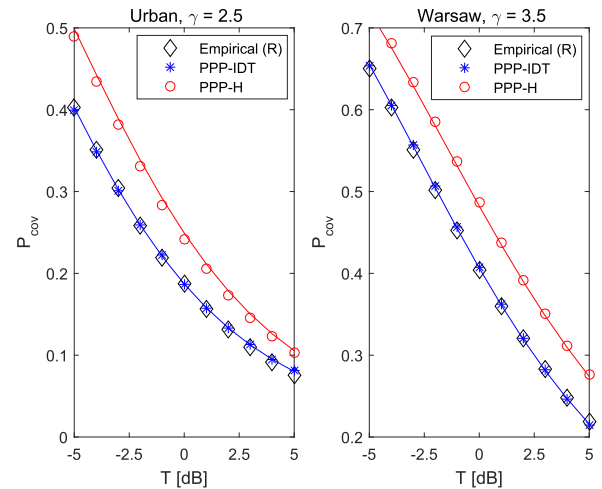


Fig. 10. P_{cov} of LGCP. Markers: Monte Carlo simulations. Solid lines: Analytical frameworks in *Theorem 1*.

locations of BSs. It is worth mentioning that these promising findings do not imply the *universal* applicability of the IDT approach to any PPs that may be available in the open technical literature. We believe, e.g., that there may exist PPs for which

the retaining probabilities to use may be different from those reported in (10) and (11). The results reported in the present paper provide, however, the indisputable evidence that the proposed IDT approach is sufficiently accurate, general, and

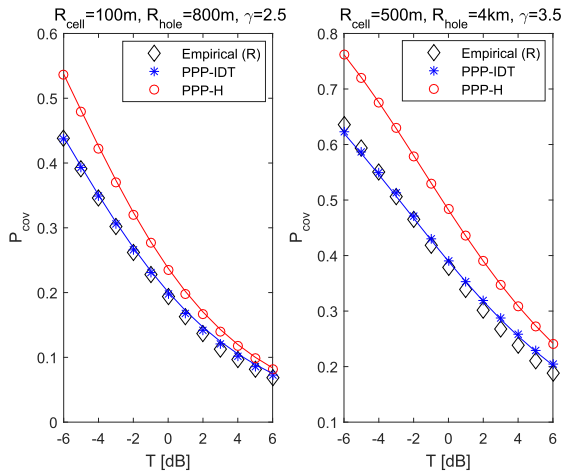


Fig. 11. P_{cov} of PHP. Markers: Monte Carlo simulations. Solid lines: Analytical frameworks in *Theorem 1*.

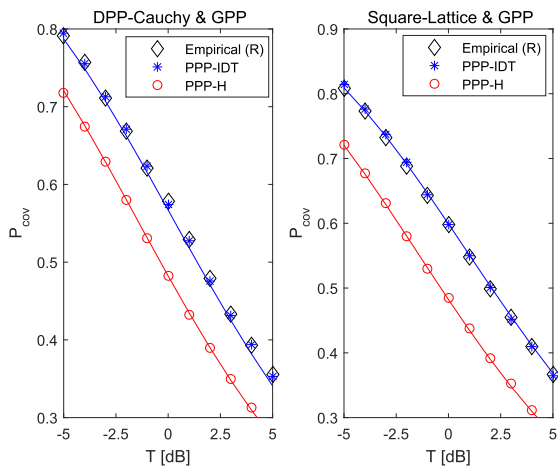


Fig. 12. P_{cov} of DPP-Cauchy (Houston) & GPP (Urban, $\beta = 0.9$) and Square-Lattice (ISD = 100 m) & GPP (Urban, $\beta = 0.9$). Setup: $\gamma = 3.5$. Markers: Monte Carlo simulations. Solid lines: Analytical frameworks in *Theorem 3*.

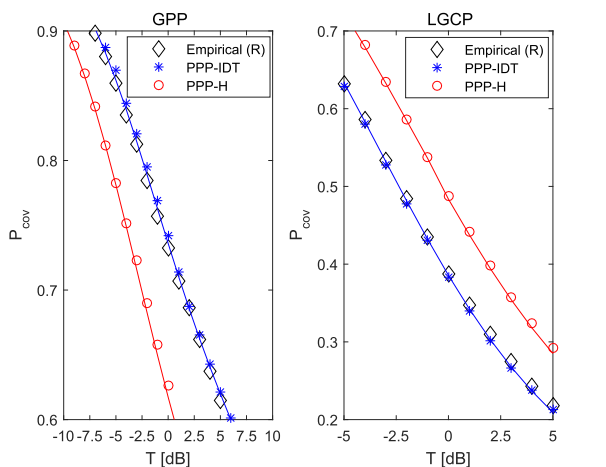


Fig. 13. P_{cov} of GPP (Urban, $\beta = 0.925$) and LGCP (Urban). Setup: $\gamma_{\text{los}} = 2.5$, $\gamma_{\text{mlos}} = 3.5$, $D_B = 109.8517$ m, $q_{\text{los}}^{(\text{in})} = 0.7196$, $q_{\text{los}}^{(\text{out})} = 0.0002$. Markers: Monte Carlo simulations. Solid lines: Analytical frameworks in *Theorem 2*.

analytically tractable for modeling, studying, and optimizing cellular network deployments whose BSs are distributed according to several empirically validated PPs.

VII. CONCLUSION

In the present paper, we have introduced a new tractable approach for modeling and analyzing cellular networks where the locations of the BSs exhibit some degree of spatial interaction, i.e., repulsion or clustering. The proposed IDT approach is based on the theory of I-PPPs, and it is shown to be tractable and insightful. Tractability and accuracy have been substantiated by using several data sets for the locations of cellular BSs that are available in the literature. The IDT approach may be applied in different ways to simplify the analysis and optimization of cellular networks. A non-exhaustive list of potential uses for system-level analysis is the following.

a) *To use it as an approximation of general PPs:* If a PP is not analytically tractable but its F-function and non-regularized K-function are available in a computable form, the IDT approach may be used to approximate the network panorama of the typical user and to obtain a tractable expression of the coverage probability that may be studied as a function of many radio access technologies.

b) *To use it as a tractable model whose parameters are obtained from empirical data:* If the PP model is unknown and the analysis can be based only on empirical data sets for the locations of the BSs, the IDT approach may be applied for system-level analysis and optimization by simply estimating the F-function and the non-regularized K-function from the empirical data set. This may be done by using the *Fest* function [44, p. 483] and the *Kest* function [44, p. 683] that are available in the *spatstat* package of the R software environment for statistical computing and graphics.

c) *To use it to simplify the computation of relevant performance metrics:* As discussed in Section IV-B, the IDT approach may be used to simplify the computation of relevant performance metrics that quantify the impact of spatial repulsion and clustering in cellular networks.

d) *To use it as a new parametric approach for modeling and optimizing cellular networks:* The IDT approach may be considered to be a spatial model on its own, which may allow one to generate PPs with different kinds of spatial interactions. The triplets of parameters (a_F, b_F, c_F) and (a_K, b_K, c_K) may not be obtained from the F-function and non-regularized K-function of other PPs, but they may be considered as free parameters as a function of which the network performance can be studied and optimized. One may compute the best triplets that optimize the coverage probability under some communication constraints and then use them for optimal network planning.

Based on these potential applications, we argue that the IDT approach may constitute an efficient alternative to employing system-level simulations for analyzing and optimizing cellular networks. The reason is that the proposed equivalent system based on I-PPPs depends only on the network geometry. This implies that the triplets of parameters that determine the spatial inhomogeneities of the equivalent network model need to be determined just once for a given network deployment, while they can be used to formulate several optimization problems in order to identify the best communication technologies and

protocols to be employed in cellular networks. Usually, this is a more efficient approach than using brute-force system-level simulations.

In conclusion, we believe that the IDT approach may have wide applicability to the modeling and design of cellular networks, e.g., to study the advantages and limitations of emerging radio access technologies by taking the spatial interactions of practical network topologies into account. There are many possible generalizations of the theories proposed in the present paper, which include, but are not limited to, the impact of different path-loss models [47], the analysis of uplink cellular networks [37], the optimization of spectral efficiency and energy efficiency [38], the analysis of the spatial correlation between the locations of BSs and MTs [48], [49].

APPENDIX A PROOF OF THEOREM 1

The proof follows by inserting (12) and (13) in (7), and by computing the integral in (8) with the aid of the following notable integrals ($v_1(x) = {}_2F_1(1, -n/\gamma, 1 - n/\gamma, x)$, $v_2(x) = {}_2F_1(1, n/\gamma, 1 + n/\gamma, x)$):

$$\begin{aligned} \mathcal{J}_1(z) &= \int_A^{+\infty} (1+t/\theta)^{-1} (z/\gamma) t^{n/\gamma-1} dt \\ &= -(z/n) A^{n/\gamma} (1 - v_1(-\theta/A)) \quad \text{for } \gamma > n \\ \mathcal{J}_2(z) &= \int_A^B (1+t/\theta)^{-1} (z/\gamma) t^{n/\gamma-1} dt \\ &= (z/n) B^{n/\gamma} v_2(-B/\theta) - (z/n) A^{n/\gamma} v_2(-A/\theta) \end{aligned} \quad (23)$$

APPENDIX B PROOF OF PROPOSITION 1

Let us consider the case study when Ψ_{BS} exhibits spatial inhibition. The case study when Ψ_{BS} exhibits spatial aggregation can be proved by using a similar line of thought and, hence, the details are omitted for brevity. By applying some changes of variable and by adopting a simpler notation for ease of writing, $\tilde{P}_{cov}^{(o)} = P_{\mathcal{I}}$ and $P_{cov}^{(H-PPP)} = P_{\mathcal{H}}$ can be written as follows:

$$\begin{aligned} P_{\mathcal{I}} &= \int_0^{+\infty} e^{-\eta\zeta^\gamma} \mathcal{M}_{\mathcal{I}}(\zeta) f_{\mathcal{I}}(\zeta) d\zeta \\ P_{\mathcal{H}} &= \int_0^{+\infty} e^{-\eta\zeta^\gamma} \mathcal{M}_{\mathcal{H}}(\zeta) f_{\mathcal{H}}(\zeta) d\zeta \end{aligned} \quad (24)$$

where $\eta = T\kappa\sigma_N^2/P_{tx}$, and the subscripts \mathcal{I} and \mathcal{H} are referred to the network models based on I-PPPs (the IDT approach) and H-PPPs, respectively. By introducing the shorthand notation $\Lambda_{\Phi_{BS}^{(\cdot)}}(\mathcal{B}(0, \zeta)) = \Lambda_{(\cdot)}(\zeta)$ and $\Lambda_{\Phi_{BS}^{(1)}}(\mathcal{B}(0, \zeta)) = \Lambda_{(\cdot)}^{(1)}(\zeta)$, the following holds: $f_{\mathcal{I}}(\zeta) = \Lambda_F^{(1)}(\zeta) \exp(-\Lambda_F(\zeta))$, $\mathcal{M}_{\mathcal{I}}(\zeta) = \exp\left(-\int_{\zeta}^{+\infty} (1 + (y/\zeta)^\gamma T^{-1})^{-1} \Lambda_K^{(1)}(y) dy\right)$, $\Lambda_{\mathcal{H}}(\zeta) = \pi\lambda_{BS}\zeta^2$, $\Lambda_{\mathcal{H}}^{(1)}(\zeta) = 2\pi\lambda_{BS}\zeta$, $f_{\mathcal{H}}(\zeta) = \Lambda_{\mathcal{H}}^{(1)}(\zeta) \times \exp(-\Lambda_{\mathcal{H}}(\zeta)) = 2\pi\lambda_{BS}\zeta \exp(-\pi\lambda_{BS}\zeta^2)$, and $\mathcal{M}_{\mathcal{H}}(\zeta) = \exp\left(-\int_{\zeta}^{+\infty} (1 + (y/\zeta)^\gamma T^{-1})^{-1} \Lambda_{\mathcal{H}}^{(1)}(y) dy\right) = \pi\lambda_{BS}\zeta^2 ({}_2F_1(1, -2/\gamma, 1 - 2/\gamma, -T) - 1)$.

If $\check{b}_K \leq \check{c}_K \leq 1$, from *Lemma 5*, we have $\Lambda_K^{(1)}(\zeta) \leq \Lambda_{\mathcal{H}}^{(1)}(\zeta)$ for $\zeta \geq 0$. This implies $\mathcal{M}_{\mathcal{I}}(\zeta) \geq \mathcal{M}_{\mathcal{H}}(\zeta)$ for $\zeta \geq 0$. As a result, the following Lower-Bound (LB) for $P_{\mathcal{I}}$ holds:

$$\begin{aligned} P_{\mathcal{I}} &\geq P_{\mathcal{I}}^{(LB)} = \int_0^{+\infty} e^{-\eta\zeta^\gamma} \mathcal{M}_{\mathcal{H}}(\zeta) f_{\mathcal{I}}(\zeta) d\zeta \\ &\stackrel{(a)}{=} \int_0^{+\infty} \left(-\chi^{(1)}(\zeta)\right) (1 - \exp(-\Lambda_F(\zeta))) d\zeta \end{aligned} \quad (25)$$

where (a) follows by applying the integration by parts formula and by introducing the functions $\chi(\zeta) = e^{-\eta\zeta^\gamma} \mathcal{M}_{\mathcal{H}}(\zeta) \geq 0$ and $\chi^{(1)}(\zeta) = d\chi(\zeta)/d\zeta \leq 0$, where the inequalities hold for $\zeta \geq 0$.

If $\check{b}_F \geq \check{c}_F \geq 1$, from *Lemma 5*, we have $\Lambda_F^{(1)}(\zeta) \geq \Lambda_{\mathcal{H}}^{(1)}(\zeta)$ for $\zeta \geq 0$. This implies $1 - \exp(-\Lambda_F(\zeta)) \geq 1 - \exp(-\Lambda_{\mathcal{H}}(\zeta))$ for $\zeta \geq 0$. As a result, the following LB for $P_{\mathcal{I}}^{(LB)}$ holds:

$$\begin{aligned} P_{\mathcal{I}} &\geq P_{\mathcal{I}}^{(LB)} = \int_0^{+\infty} \left(-\chi^{(1)}(\zeta)\right) (1 - e^{-\Lambda_F(\zeta)}) d\zeta \\ &\geq \int_0^{+\infty} \left(-\chi^{(1)}(\zeta)\right) (1 - e^{-\Lambda_{\mathcal{H}}(\zeta)}) d\zeta \\ &\stackrel{(b)}{=} P_{\mathcal{H}} \end{aligned} \quad (26)$$

where (b) follows from $P_{\mathcal{H}}$ in (24) by applying the integration by parts formula similar to (a) in (25). In summary, the condition $P_{\mathcal{I}} \geq P_{\mathcal{H}}$ is proved.

REFERENCES

- [1] J. G. Andrews, F. Baccelli, and R. K. Ganti, "A tractable approach to coverage and rate in cellular networks," *IEEE Trans. Commun.*, vol. 59, no. 11, pp. 3122–3134, Nov. 2011.
- [2] H. S. Dhillon, R. K. Ganti, F. Baccelli, and J. G. Andrews, "Modeling and analysis of K-tier downlink heterogeneous cellular networks," *IEEE J. Sel. Areas Commun.*, vol. 30, no. 3, pp. 550–560, Apr. 2012.
- [3] M. Di Renzo, A. Guidotti, and G. E. Corazza, "Average rate of downlink heterogeneous cellular networks over generalized fading channels: A stochastic geometry approach," *IEEE Trans. Commun.*, vol. 61, no. 7, pp. 3050–3071, Jul. 2013.
- [4] H. S. Dhillon, M. Kountouris, and J. G. Andrews, "Downlink MIMO HetNets: Modeling, ordering results and performance analysis," *IEEE Trans. Wireless Commun.*, vol. 12, no. 10, pp. 5208–5222, Oct. 2013.
- [5] M. Di Renzo and W. Lu, "Stochastic geometry modeling and performance evaluation of MIMO cellular networks using the equivalent-in-distribution (EiD)-based approach," *IEEE Trans. Commun.*, vol. 63, no. 3, pp. 977–996, Mar. 2015.
- [6] T. Bai and R. W. Heath, Jr., "Coverage and rate analysis for millimeter-wave cellular networks," *IEEE Trans. Wireless Commun.*, vol. 14, no. 2, pp. 1100–1114, Feb. 2015.
- [7] M. Di Renzo, "Stochastic geometry modeling and analysis of multi-tier millimeter wave cellular networks," *IEEE Trans. Wireless Commun.*, vol. 14, no. 9, pp. 5038–5057, Sep. 2015.
- [8] T. Bai and R. W. Heath, Jr., "Analyzing uplink SINR and rate in massive MIMO systems using stochastic geometry," *IEEE Trans. Commun.*, vol. 64, no. 11, pp. 4592–4606, Nov. 2016.
- [9] M. Di Renzo, W. Lu, and P. Guan, "The intensity matching approach: A tractable stochastic geometry approximation to system-level analysis of cellular networks," *IEEE Trans. Wireless Commun.*, vol. 15, no. 9, pp. 5963–5983, Sep. 2016.
- [10] W. Lu and M. Di Renzo, "Stochastic geometry modeling of cellular networks: Analysis, simulation and experimental validation," in *Proc. ACM MSWiM*, Nov. 2015, pp. 179–188.
- [11] M. Haenggi, J. G. Andrews, F. Baccelli, O. Dousse, and M. Franceschetti, "Stochastic geometry and random graphs for the analysis and design of wireless networks," *IEEE J. Sel. Areas Commun.*, vol. 27, no. 7, pp. 1029–1046, Sep. 2009.

- [12] H. ElSawy, E. Hossain, and M. Haenggi, “Stochastic geometry for modeling, analysis, and design of multi-tier and cognitive cellular wireless networks: A survey,” *IEEE Commun. Surveys Tuts.*, vol. 15, no. 3, pp. 996–1019, 3rd Quart., 2013.
- [13] H. ElSawy, A. Sultan-Salem, M. S. Alouini, and M. Z. Win, “Modeling and analysis of cellular networks using stochastic geometry: A tutorial,” *IEEE Commun. Surveys Tuts.*, vol. 19, no. 1, pp. 167–203, 1st Quart., 2017.
- [14] J. G. Andrews, A. K. Gupta, and H. S. Dhillon. (Oct. 2016). “A primer on cellular network analysis using stochastic geometry.” [Online]. Available: <https://arxiv.org/abs/1604.03183>
- [15] A. Guo and M. Haenggi, “Spatial stochastic models and metrics for the structure of base stations in cellular networks,” *IEEE Trans. Wireless Commun.*, vol. 12, no. 11, pp. 5800–5812, Nov. 2013.
- [16] N. Deng, W. Zhou, and M. Haenggi, “Heterogeneous cellular network models with dependence,” *IEEE J. Sel. Areas Commun.*, vol. 33, no. 10, pp. 2167–2181, Oct. 2015.
- [17] A. M. Ibrahim, T. ElBatt, and A. El-Keyi, “Coverage probability analysis for wireless networks using repulsive point processes,” in *Proc. IEEE 24th Int. Symp. Pers. Indoor Mobile Radio Commun. (PIMRC)*, Sep. 2013, pp. 1002–1007.
- [18] M. Haenggi, “The mean interference-to-signal ratio and its key role in cellular and amorphous networks,” *IEEE Wireless Commun. Lett.*, vol. 3, no. 6, pp. 597–600, Dec. 2014.
- [19] M. Haenggi, “ASAPPP: A simple approximative analysis framework for heterogeneous cellular networks,” in *Proc. IEEE Int. Workshop Heterogeneous Small Cell Nets.*, Dec. 2014. [Online]. Available: <https://www3.nd.edu/mhaenggi/talks/hetsnets14.pdf>
- [20] N. Deng, W. Zhou, and M. Haenggi, “The Ginibre point process as a model for wireless networks with repulsion,” *IEEE Trans. Wireless Commun.*, vol. 14, no. 1, pp. 107–121, Jan. 2015.
- [21] A. Guo and M. Haenggi, “Asymptotic deployment gain: A simple approach to characterize the SINR distribution in general cellular networks,” *IEEE Trans. Commun.*, vol. 63, no. 3, pp. 962–976, Mar. 2015.
- [22] J. S. Gomez, A. Vasseur, A. Vergne, P. Martins, L. Decreusefond, and W. Chen. “A case study on regularity in cellular network deployment,” *IEEE Wireless Commun. Lett.*, vol. 4, no. 4, pp. 421–424, Aug. 2015.
- [23] Y. Li, F. Baccelli, H. S. Dhillon, and J. G. Andrews, “Statistical modeling and probabilistic analysis of cellular networks with determinantal point processes,” *IEEE Trans. Commun.*, vol. 63, no. 9, pp. 3405–3422, Sep. 2015.
- [24] H. Wei, N. Deng, W. Zhou, and M. Haenggi, “Approximate SIR analysis in general heterogeneous cellular networks,” *IEEE Trans. Commun.*, vol. 64, no. 3, pp. 1259–1273, Mar. 2016.
- [25] R. K. Ganti and M. Haenggi, “Asymptotics and approximation of the SIR distribution in general cellular networks,” *IEEE Trans. Wireless Commun.*, vol. 15, no. 3, pp. 2130–2143, Mar. 2016.
- [26] Z. Yazdanshenasan, H. S. Dhillon, M. Afshang, and P. H. J. Chong, “Poisson hole process: Theory and applications to wireless networks,” *IEEE Trans. Wireless Commun.*, vol. 15, no. 11, pp. 7531–7546, Nov. 2016.
- [27] J. Kibilda, B. Galkin, and L. A. DaSilva, “Modelling multi-operator base station deployment patterns in cellular networks,” *IEEE Trans. Mobile Comput.*, vol. 15, no. 12, pp. 3087–3099, Dec. 2016.
- [28] C.-S. Choi, J. O. Woo, and J. G. Andrews, “An analytical framework for modeling a spatially repulsive cellular network,” *IEEE Trans. Commun.*, vol. 66, no. 2, pp. 862–874, Feb. 2018.
- [29] C. Saha, M. Afshang, and H. S. Dhillon, “3GPP-inspired HetNet model using Poisson cluster process: Sum-product functionals and downlink coverage,” *IEEE Trans. Commun.*, vol. 66, no. 5, pp. 2219–2234, May 2018.
- [30] A. Baddeley, E. Rubak, and R. Turner, *Spatial Point Patterns: Methodology and Applications With R*. London, U.K.: Chapman & Hall, Nov. 2015.
- [31] U. Schilcher, G. Brandner, and C. Bettstetter, “Quantifying inhomogeneity of spatial point patterns,” *Comput. Netw.*, vol. 115, pp. 65–81, Mar. 2017.
- [32] R. L. Streit, *Poisson Point Processes: Imaging, Tracking, and Sensing*. New York, NY, USA: Springer-Verlag, Sep. 2010.
- [33] M. Haenggi, “User point processes in cellular networks,” *IEEE Wireless Commun. Lett.*, vol. 6, no. 2, pp. 258–261, Apr. 2017.
- [34] Y. Wang, M. Haenggi, and Z. Tan, “The meta distribution of the SIR for cellular networks with power control,” *IEEE Trans. Commun.*, vol. 66, no. 4, pp. 1745–1757, Apr. 2018.
- [35] F. Baccelli and B. Błaszczyszyn, *Stochastic Geometry and Wireless Networks, Part I: Theory*. Hanover, MA, USA: Now, Sep. 2009.
- [36] M. Haenggi, *Stochastic Geometry for Wireless Networks*. Cambridge, U.K.: Cambridge Univ. Press, Nov. 2012.
- [37] M. Di Renzo and P. Guan, “Stochastic geometry modeling and system-level analysis of uplink heterogeneous cellular networks with multi-antenna base stations,” *IEEE Trans. Commun.*, vol. 64, no. 6, pp. 2453–2476, Jun. 2016.
- [38] M. Di Renzo, A. Zappone, T. T. Lam, and M. Debbah, “System-level modeling and optimization of the energy efficiency in cellular networks—A stochastic geometry framework,” *IEEE Trans. Wireless Commun.*, vol. 17, no. 4, pp. 2539–2556, Apr. 2018.
- [39] B. Błaszczyszyn, M. K. Karray, and H. P. Keeler, “Using Poisson processes to model lattice cellular networks,” in *Proc. IEEE INFOCOM*, Apr. 2013, pp. 773–781.
- [40] J. Lee and C. Tepedelenlioğlu, “Stochastic ordering of interference in large-scale wireless networks,” *IEEE Trans. Signal Process.*, vol. 62, no. 3, pp. 729–740, Feb. 2014.
- [41] F. Lavancier, J. Møller, and E. Rubak, “Determinantal point process models and statistical inference,” *J. Roy. Stat. Soc., Ser. B, Stat. Methodol.*, vol. 77, no. 4, pp. 853–877, Sep. 2015.
- [42] D. Moltchanov, “Distance distributions in random networks,” *Ad Hoc Netw.*, vol. 10, no. 6, pp. 1146–1166, 2012.
- [43] J. Møller, A. R. Syversveen, and R. P. Waagepetersen, “Log Gaussian Cox processes,” *Scand. J. Statist.*, vol. 25, no. 3, pp. 451–482, Sep. 1998.
- [44] A. Baddeley *et al.*, “SPATSTAT: Spatial point pattern analysis, model-fitting, simulation, tests,” in *The Comprehensive R Archive Network*, Jan. 2018. [Online]. Available: <https://cran.r-project.org/web/packages/spatstat/spatstat.pdf>
- [45] M. Afshang, C. Saha, and H. S. Dhillon, “Nearest-neighbor and contact distance distributions for Matérn cluster process,” *IEEE Commun. Lett.*, vol. 21, no. 12, pp. 2686–2689, Dec. 2017.
- [46] L. Decreusefond, I. Flint, and I. F. A. Vergne, “A note on the simulation of the Ginibre point process,” *J. Appl. Probab.*, vol. 52, no. 4, pp. 1003–1012, 2015.
- [47] A. AlAmmouri, J. G. Andrews, and F. Baccelli, “SINR and throughput of dense cellular networks with stretched exponential path loss,” *IEEE Trans. Wireless Commun.*, vol. 17, no. 2, pp. 1147–1160, Feb. 2018. [Online]. Available: <https://arxiv.org/abs/1703.08246>
- [48] M. Mirahsan, R. Schoenen, and H. Yanikomeroglu, “HetHetNets: Heterogeneous traffic distribution in heterogeneous wireless cellular networks,” *IEEE J. Sel. Areas Commun.*, vol. 33, no. 10, pp. 2252–2265, Oct. 2015.
- [49] C. Saha, M. Afshang, and H. S. Dhillon, “Enriched K -tier HetNet model to enable the analysis of user-centric small cell deployments,” *IEEE Trans. Wireless Commun.*, vol. 16, no. 3, pp. 1593–1608, Mar. 2017.



Marco Di Renzo (S’05–AM’07–M’09–SM’14) was born in L’Aquila, Italy, in 1978. He received the Laurea (*cum laude*) and the Ph.D. degrees in electrical engineering from the University of L’Aquila, Italy, in 2003 and 2007, respectively, and the D.Sc. degree (HDR) from the University Paris-Sud, France, in 2013. Since 2010, he has been a CNRS Associate Professor (“Chargé de Recherche Titulaire CNRS”) with the Laboratory of Signals and Systems, Paris-Saclay University—CNRS, CentraleSupélec, Univ Paris Sud, Paris, France. He is

currently an Adjunct Professor with the University of Technology Sydney, Australia, a Visiting Professor with the University of L’Aquila, Italy, and a Co-Founder of the university spin-off company—WEST Aquila s.r.l., Italy. He is a Distinguished Lecturer of the IEEE Vehicular Technology Society and the IEEE Communications Society. He is the Project Coordinator of the European-funded projects H2020-MSCA ETN-5Gwireless and H2020-MSCA ETN-5Gaura. He was a recipient of several awards, including the 2013 IEEE-COMSOC Best Young Researcher Award for Europe, Middle East, and Africa (EMEA Region), the 2013 NoE-NEWCOM# Best Paper Award, the 2014–2015 Royal Academy of Engineering Distinguished Visiting Fellowship, the 2015 IEEE Jack Neubauer Memorial Best System Paper Award, the 2015–2018 CNRS Award for Excellence in Research and in Advising Doctoral Students, the 2016 MSCA Global Fellowship (declined), the 2017 SEE-IEEE Alain Glavieux Award, the 2018 IEEE ICNC Silver Contribution Award, and six best paper awards at the IEEE conferences (the 2012 and 2014 IEEE CAMAD, the 2013 IEEE VTC-Fall, the 2014 IEEE ATC, the 2015 IEEE ComManTel, and 2017 IEEE SigTelCom). He serves as the Associate Editor-in-Chief for the IEEE COMMUNICATIONS LETTERS and an Editor for the IEEE TRANSACTIONS ON COMMUNICATIONS and the IEEE TRANSACTIONS ON WIRELESS COMMUNICATIONS.



Her research interests include wireless communications and stochastic geometry.

Shanshan Wang was born in Nanjing, China, in 1991. She received the B.Sc. degree in communications engineering from Soochow University, Suzhou, China, in 2013, and the M.Sc. degree (Hons.) in wireless communication and signal processing from the University of Bristol, Bristol, U.K., in 2014. She is currently pursuing the Ph.D. degree with the Laboratory of Signals and Systems, Paris-Saclay University, Paris, France. She is currently an Early Stage Researcher of the European-funded project MSCA ETN-5Gwireless.



include wireless communications and stochastic geometry.

Xiaojun Xi was born in Shanghai, China, in 1991. He received the B.Sc. degree in electronic and information engineering from the Nanjing University of Science and Technology, China, in 2014, and the M.Sc. degree (Hons.) in signal processing and communications from The University of Edinburgh, U.K., in 2015. He is currently pursuing the Ph.D. degree with the Laboratory of Signals and Systems, Paris-Saclay University, Paris, France. He is also an Early Stage Researcher of the European-funded project MSCA ITN-5Gaura. His research interests